Materials & Design 256 (2025) 114240

Contents lists available at ScienceDirect

Materials & Design

journal homepage: www.elsevier.com/locate/matdes

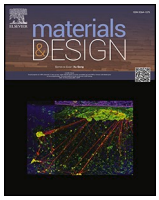

Direct monitoring of intracellular polymer degradation via BODIPY dynamic dequenching

Justine Bassil [a,b], Mohamed A.M. Kamal [a,b], Aljoscha Gabelmann [a,b], Anastasia Christoulaki [c], Marcus Koch [d], Mostafa M. Hamed [a,b], Brigitta Loretz [a], Markus Gallei [e,f], Eric Buhler [c], Claus-Michael Lehr [a,b], Anna K.H. Hirsch [a,b,*], Sangeun Lee [a,b,*]

[a] Helmholtz Institute of Pharmaceutical Research Saarland (HIPS) – Helmholtz Centre for Infection Research (HZI), Campus E 8.1, 66123 Saarbrücken, Germany
[b] Department of Pharmacy, PharmaScienceHub, Saarland University, Campus C4. 1, 66123 Saarbrücken, Germany
[c] Laboratoire Matière et Systèmes Complexes (MSC), UMR 7057, Université Paris Cité, Physics Department, Bâtiment Condorcet, 75013 Paris, France
[d] INM-Leibniz Institute for New Materials, Campus D2 2, 66123 Saarbrücken, Germany
[e] Polymer Chemistry, Campus C4 2, 66123 Saarbrücken, Germany
[f] Saarene, Saarland Center for Energy Materials and Sustainability, Campus C4 2, 66123 Saarbrücken, Germany

ARTICLE INFO

Keywords:
Biodegradable polymer
Biodynamers
Fluorescent labeling
BODIPY

ABSTRACT

Biodegradable polymers play a crucial role in biomedical applications, particularly as nanocarriers in drug delivery. While labeling the polymers with fluorescent dyes facilitates monitoring their biodistribution and post cellular uptake, tracking polymer degradation within biological systems remains a challenge. This raises important unanswered questions regarding the fate of the polymers, their degradation products, and the degree of their degradation within biological systems. In this study, we developed a novel dynamic biodynamer (BDP-Lys) composed of BODIPY and lysine-hydrazide monomers linked by reversible dynamic covalent bonds, designed to control the fluorescence of BODIPY by degradation. The BDP-Lys undergoes pH-responsive degradation, leading to recovery of quenched BODIPY and enhanced fluorescence emissions, thereby enabling direct monitoring of intracellular polymer degradation. Physicochemical characterization revealed its molecular weight, filament-like morphology, and a notable 12-fold increase in fluorescence intensity at acid-induced degradation. *In vitro* studies demonstrated excellent biocompatibility, efficient cellular uptake and a threefold increase in fluorescence due to polymer degradation in mammalian cells, resulting in a maximum of 17 % monomer release in the first 24 h. Thus, BDP-Lys emerges as a promising tool for exploring polymer behavior in biological systems, providing real-time insights into degradation and offering new opportunities to address unresolved questions in the field.

1. Introduction

Biodegradable and biocompatible polymers have attracted significant attention, emerging as a prominent area of research in drug delivery and biomedical applications, due to their adaptable functional properties in biological environments. Such polymers often serve as nanocarriers capable of encapsulating, protecting, delivering, and releasing various therapeutic agents in a controlled and targeted manner [1–4]. Labeling of these nanocarriers using imaging agents like fluorescent dyes enables the monitoring of their biodistribution and cellular uptake within the tissues, making them available in biological studies and diagnostics [5,6].

Most current fluorescent labeling techniques are achieved through chemical dye conjugation to polymeric carriers or direct encapsulation of dyes in nanocarriers during particle formation [7–10]. However, it is important to note the limitations of both labeling approaches. For instance, while encapsulation of fluorescent dyes allows monitoring of dye release, it also poses risks of uncontrollable leakage and quenching, potentially affecting biodistribution and altering the interpretation of polymer breakdown [7,11]. More importantly, the release of encapsulated dye is often associated with dissociation or disassembly of the polymeric nanocarriers as a consequence of polymer degradation. Thus, the real-time tracking of the degradation process with this approach is highly challenging or most likely impossible, as it is difficult to

* Corresponding authors.
E-mail addresses: anna.hirsch@helmholtz-hips.de (A.K.H. Hirsch), Sangeun.Lee@uni-saaland.de (S. Lee).

https://doi.org/10.1016/j.matdes.2025.114240
Received 27 March 2025; Received in revised form 11 June 2025; Accepted 12 June 2025
Available online 14 June 2025

distinguish between polymer breakdown and nanocarrier disassembly [10,12,13], and few study [14] effectively monitor and track polymer breakdown *in situ* within biological systems.

Covalent dye conjugation offers theoretically the most stable labeling, provided that the dye remains attached during polymer degradation. Nonetheless, fluorescence imaging or measurements primarily tracks the fluorescence signal of the dye, making it difficult to distinguish whether the signal originates from the nanoparticle, the polymer itself, or the released dye, which complicates the interpretation of such data [15,16]. Typically, it is recommended to keep fluorescent labels within a weight percentage of 0.1–5 % of the polymer in order to minimize structural changes and effects of polymer degradation. Another argument is to avoid changes in Corona formation and nano-bio interactions of such drug carriers [17,18]. Regardless of molecular weight of dye covalent labeling there are still challenges in accurately assessing polymer breakdown and accumulation, especially after exposure to biological systems, as various degradation pathways can occur without affecting any of the labeled units; whether it is through breaking bonds along the polymer chain or removing monomers from ends. Moreover, the presence of the conjugated dye can alter the degradation of the polymer, potentially affecting both in-chain and end-chain degradation mechanisms such as hydrolysis, oxidation, or enzymatic cleavage [15,19,20].

Concerns regarding the biocompatibility and potential toxicity of the dyes or the degraded polymers before or after degradation might arise and further complicate their interaction and application *in vivo* [21,22]. Although the stability, toxicity, and leakage issues of the labeling methods are frequently evaluated [23–25], each study employs different nanoparticles and techniques for individual dyes, making it challenging to identify the best strategy for particle labeling preparation with the desired fluorescent properties. Thus, while fluorescent labeling of polymeric carriers or its encapsulated cargo is convenient for initial biodistribution studies, it does not provide insight into polymer degradation, accumulation, and fate following cellular uptake. This highlights the need for new approaches to effectively monitor these processes.

Biodynamers have emerged from the application of constitutionally dynamic chemistry to polymer science, with their polymerization occurring through reversible dynamic covalent bonds (DCB), most often imines and acylhydrazone bonds [26,27]. They undergo spontaneous physical and chemical modification via bond forming, bond breaking, and exchange of biological inspired monomers under specific conditions. As a result, the inherent properties of biomolecular monomers and reversible DCB equip biodynamers with numerous advantages such as biocompatibility, biodegradability, biofunctionality, tuneability, and self-healing capabilities, making them the ideal stimuli-responsive materials for versatile applications in the biomedical field, particularly as polymers for nanocarriers [28,29].

In our previous studies, we reported a carbazole-based biodynamer (CA-Lys) composed of water-soluble carbazole dicarboxaldehyde (CA) and lysine hydrazide, which exhibits significant pH-dependent changes in both morphology and fluorescence properties [30]. Upon polymerization, the spherical micelles of the CA monomer transformed into rigid nanorods, accompanied by a pronounced redshift in fluorescence emission as the pH increases from pH 3 to pH 13. This shift is attributed to the protonation effects on the carbazole fluorophores, which alter their conjugated systems and optical properties [30]. Consequently, both polymerization and pH changes impact fluorescence intensity and spectral characteristics, highlighting the complex interplay between pH, morphology, and optical behavior in biodynamers.

In this context, the controlled integration of fluorescent dyes into the biodynamers offers a promising approach to gain insight into the degradation and fate of polymers. Herein, we present a novel biodynamer (BDP-Lys) capable of monitoring intracellular polymer degradation. The BDP-Lys was designed to dynamically reactivate and enhance fluorescence emission upon degradation under acidic environments within cells. It is composed of two key monomers: on one hand, BODIPY-dialdehydes (BDP), consisting of a hydrophobic and fluorescent aromatic core and a hydrophilic hexaethylene glycol (HG) chain on its *meso*-position, and on the other hand, lysine hydrazides (Lys). BODIPY, known for their fluorescence properties, offers a high fluorescence quantum yield, sharp emission/absorption in UV–visible range that is barely affected by pH environment [31,32] low toxicity, and is widely used in bioimaging and sensors applications [33,34]. Conversely, lysine hydrazide, a derivative of an amino acid, serves as a versatile building block with pharmaceutical applications [35]. First, we report the design and synthesis of BDP-Lys, followed by investigating its characteristics in terms of size, morphology, optical, and pH-responsive behavior using several physical methods. Next, we evaluated its compatibility with mammalian cells and performed the first studies for cellular uptake, and *in situ* degradation within the cells.

2. Materials and methods

2.1. General

Reagents and dry solvents like dimethylformamide (DMF), dichloromethane (DCM) and dichloroethane (DCE) were purchased from the highest commercial sources and used as received, unless otherwise stated. Normal solvents were purchased as technical grade and used as received. Lysine methyl ester (H-Lys-OMe.2HCl) was purchased from Fluorochem Ltd. (Karlsruhe, Germany). All air- or moisture-sensitive reactions were carried out in dried solvents and in oven-dried glassware (>100 °C) under an atmosphere of nitrogen or argon. Thin layer chromatography (TLC) was performed with 0.25 mm E. Merck silica plates 60F-254, with a suitable solvent system and was visualized using UV fluorescence (254 and 366 nm).

Purification of the products was done via Column chromatography using either the automated flash chromatography system (normal phase) CombiFlash Rf+ (Teledyne Isco, Lincoln, NE, USA) equipped with RediSepRf silica columns (Axel Semrau, Sprockhövel Germany), or the automated flash chromatography system (reversed phase) Pure C-850 Flashprep (BUCHI, Switzerland) equipped with TELOS C18 flash columns.

Product purity was determined by: 1) Liquid chromatography-mass spectrometry (LC-MS) system, featuring a Dionex UltiMate 3000 pump, autosampler, column compartment and MWD or DAD detector (Thermo Fisher Scientific, Dreieich, Germany) and ESI quadrupole MS (MSQ Plus or ISQ EC, Thermo Fisher Scientific, Dreieich, Germany). Columns used: a) Hypersil Gold column, 100 x 2.1 mm, 3 μm. At a flow rate of 700 μL/min, the gradient of water (H_2O) + 0.1 % formic acid (FA) and acetonitrile (ACN) + 0.1 % FA starting from 5 % ACN and then increased to 100 % over 7 min. b) Hypersil Gold column, 100 x 1.9 mm, 2.1 μm. At a flow rate of 600 μL/min, the gradient of H_2O + 0.1 % FA and ACN + 0.1 % FA started from 5 % ACN and then increased to 100 % over 5.5 min. The mass spectrum was measured in positive and negative mode in a range from 100–1000 *m/z*. 2) High-resolution mass spectra (HR-MS) were recorded with a ThermoScientific system where a Dionex Ultimate 3000 RSLC was coupled to a Q Exactive Focus mass spectrometer with an electrospray ion (ESI) source. An Acquity UPLC® BEH C8, 150 x 2.1 mm, 1.7 μm column equipped with a VanGuard Pre-Column BEH C8, 5 x 2.1 mm, 1.7 μm (Waters, Germany) was used for separation. At a flow rate of 250 μL/min, the gradient of (A) H_2O + 0.1 % FA and (B) ACN + 0.1 % FA was held at 10 % B for 1 min and then increased to 95 % B over 4 min. The mass spectrum was measured in positive mode in a range from 120–1000 *m/z*.

Proton (^1H) and carbon (^{13}C) nuclear magnetic resonance (NMR) spectra were recorded on a Bruker Avance Neo 500 MHz spectrometer (^1H at 500.0 MHz; ^{13}C at 126.0 MHz) using deuterated solvents as an internal reference (Chloroform ($CDCl_3$): 7.26 ppm ^1H NMR, 77.2 ppm ^{13}C NMR; Dimethyl sulfoxide (DMSO-d_6): 2.50 ppm ^1H NMR, 39.5 ppm ^{13}C NMR). The chemical shifts are recorded in parts per million (ppm) and the coupling constants (J) in Hertz (Hz). The following

abbreviations were used for NMR peaks multiplicities (s: singlet, br s: broad singlet, d: doublet, dd: doublet of doublets, t: triplet, q: quartet, m: multiplet).

2.2. Synthesis of monomers and polymer BDP-Lys

*2,5,8,11,14,17-hexaoxanonadecan-19-yl4-methylbenzenesulfonate (**1**).*

The general procedure for the synthesis of **1** was modified according to literature [36]. A solution of hexaethyleneglycolmonomethylether (2.5 g, 8.44 mmol) and trimethylamine (TEA) (1.35 mL, 9.7 mmol) in dry DCM (10 mL) was set stirring in an ice bath, and a solution of tosyl chloride (1.69 g, 8.86 mmol) in dry DCM (20 mL) was added dropwise over a period of 20 min (min). The ice bath was then removed, and the reaction was stirred at room temperature (r.t.) for 14 h (h) followed by the addition of a 1 M hydrochloric acid solution (20 mL) and H_2O (30 mL). The resulting mixture was extracted with DCM. The organic phase was washed with brine (50 mL), dried over sodium sulfate (Na_2SO_4), filtered and concentrated to a yellow oil, which was subject to automated flash chromatography (DCM/methanol (MeOH), 100/0 → 95/5), yielding as a product a colorless oil (3 g, 79 %). **^{1}H NMR** (500 MHz, $CDCl_3$) δ 7.78 (d, J = 8.2 Hz, 2H), 7.33 (d, J = 8.4 Hz, 2H), 4.14 (t, J = 9.7 Hz, 2H), 3.68–3.53 (m, 22H), 3.36 (s, 3H), 2.43 (s, 3H). **^{13}C NMR** (126 MHz, $CDCl_3$) δ 144.89, 133.11, 129.92, 128.08, 72.03–68.77, 59.13, 21.74. **LC-MS** calculated (calcd) for $C_{20}H_{35}O_9S$ $[M + H]^+$: 451.20, found 451.30.

*4-((2,5,8,11,14,17-hexaoxanonadecan-19-yl)oxy)benzaldehyde (**2**).*

The synthesis of compound **2** was performed according to literature [37]. To a solution of 4-hydroxybenzylaldehyde (500 mg, 4.09 mmol) and tosyl group **(1)** (1.84 g, 4.09 mmol) in 20 mL dry DMF were added caesium carbonate (Cs_2CO_3) (4.34 g, 13.31 mmol) and sodium iodide (NaI) (6.14 mg, 40.94 μmol). The reaction mixture was stirred at r.t. overnight. Then, H_2O was added, and the resulting mixture was extracted with EtOAc. The organic layer was dried over Na_2SO_4, filtered and concentrated under reduced pressure. The crude product was purified via automated flash chromatography (DCM/MeOH, 100/0 → 90/10) affording the desired product **2** (1.4 g, 85 %) as a yellow oil. **^{1}H NMR** (500 MHz, $CDCl_3$) δ 9.88 (s, 1H), 7.82 (d, J = 6.8 Hz, 2H), 7.02 (d, J = 8.7 Hz, 2H), 4.23–4.19 (m, 2H), 3.90–3.87 (m, 2H), 3.73–3.53 (m, 20H), 3.37 (s, 3H). **^{13}C NMR** (126 MHz, $CDCl_3$) δ 190.66, 163.71, 131.80, 129.89, 114.73, 71.78, 70.76, 70.48–70.36, 69.32. **LC-MS** calcd for $C_{20}H_{33}O_8$ $[M + H]^+$: 401.22, found 401.43.

The synthesis of compounds **3**, **4**, and BDP monomer was carried out following literature procedures with some modifications [38].

*10-(4-((2,5,8,11,14,17-hexaoxanonadecan-19-yl)oxy)phenyl)-5,5-difluoro-1,3,7,9-tetramethyl-5H-4 l4,5l4-dipyrrolo[1,2-c:2′,1′-f][1,2,3]diazaborinine (**3**).*

To a heat dried Schlenk tube equipped with a magnetic stirring bar, the corresponding aldehyde **2** (850.0 mg, 2.12 mmol) and 2,4-dimethyl-1*H*-pyrrole (444.3 mg, 4.67 mmol) were dissolved in 60 mL dry DCM under nitrogen atmosphere. Trifluoroacetic acid (TFA) (185.2 μL, 2.42 mmol) was added and the resulting mixture was stirred overnight at r.t. in the dark. After complete consumption of the aldehyde, which was monitored on LC-MS, Dichloro-5,6-dicyano-1,4-benzoquinone (DDQ) (578.2 mg, 2.55 mmol) was added, and the reaction was stirred for an additional 1 h. Then, TEA (2.2 mL, 12.74 mmol) and boron trifluoride etherate ($BF_3{\cdot}Et_2O$) (2.2 mL, 17.91 mmol) were added and mixture left to stir at r.t. for another 1 h. The resulting crude was concentrated in vacuum and purified via automated flash chromatography (DCM/MeOH, 100/0 → 90/10) affording a reddish fluorescent solid (500 mg, 38 %). **^{1}H NMR** (500 MHz, $CDCl_3$) δ 7.15 (d, J = 8.5 Hz, 2H), 7.02 (d, J = 8.5 Hz, 2H), 5.97 (s, 2H), 4.18 (t, J = 4.7 Hz, 2H), 3.90 (t, J = 4.7 Hz, 2H), 3.75–3.56 (m, 20H), 3.37 (s, 3H), 2.54 (s, 6H), 1.42 (s, 6H). **^{13}C NMR** (126 MHz, $CDCl_3$) δ 159.75, 155.64, 143.55, 142.21, 132.22, 129.55, 127.60, 121.49, 115.57, 72.33, 71.30, 70.98 (m), 70.13, 67.88, 59.44, 14.99. **HRMS** calcd for $C_{32}H_{44}BF_2N_2O_7$ $[M-H]^-$: 617.32151, 617.3226.

*10-(4-((2,5,8,11,14,17-hexaoxanonadecan-19-yl)oxy)phenyl)-5,5-difluoro-1,3,7,9-tetramethyl-5H-5 l4,6l4-dipyrrolo[1,2-c:2′,1′-f][1,2,3]diazaborinine-2-carbaldehyde (**4**).*

Under nitrogen atmosphere, phosphoryl chloride ($POCl_3$) (11.4 mL, 122.80 mmol) was added dropwise to dry DMF (11.3 mL, 146.56 mmol) while maintaining the temperature below 25 °C (cooling in an ice bath). After complete addition, the mixture was stirred for 30 min at r.t. Compound **3** (490 mg, 0.792 mmol) was dissolved in 60 mL dry DCE, and carefully added. The temperature was raised to 50 °C and the reaction mixture was stirred for 2 h. After cooling to r.t., the mixture was slowly poured into a cooled sat. aq. solution of sodium bicarbonate ($NaHCO_3$) (100 mL) and further stirred for 60 min. Then, H_2O (20 mL) was added, and the resulting mixture was extracted with DCM (3 x 50 mL). The combined organic phases were dried over Na_2SO_4, filtered and solvents were removed under vacuum. The crude product was subject to an automated flash chromatography (DCM/MeOH, 100/0 → 90/10) yielding **4** (410 mg, 80 %) as a red fluorescent solid. **^{1}H NMR** (500 MHz, $CDCl_3$) δ 10.00 (s, 1H), 7.15 (d, J = 8.5 Hz, 2H), 7.05 (d, J = 8.5 Hz, 2H), 6.13 (s, 1H), 4.19 (t, J = 4.7, 2H), 3.91 (t, J = 4.7 Hz, 2H), 3.75– 3.62 (m, 20H), 3.36 (s, 3H), 2.80 (s, 3H), 2.60 (s, 3H), 1.70 (s, 3H), 1.46 (s, 3H). **^{13}C NMR** (126 MHz, $CDCl_3$) δ 185.95, 161.42, 159.81, 156.38, 147.35, 143.74, 142.89, 134.49, 130.18, 128.98, 126.26, 123.90, 115.53, 71.92, 70.65–70.53, 69.69, 67.58, 59.05, 15.10, 13.02, 11.81. **HRMS** calcd for $C_{33}H_{46}BF_2N_2O_8$ $[M + H]+$: 647.3304 found 647.3314.

*10-(4-((2,5,8,11,14,17-hexaoxanonadecan-19-yl)oxy)phenyl)-5,5-difluoro-1,3,7,9-tetramethyl-5H-4 l4,5l4-dipyrrolo[1,2-c:2′,1′-f][1,2,3]diazaborinine-2,8-dicarbaldehyde (**BDP**).*

Under nitrogen atmosphere, $POCl_3$ (8.9 mL, 95.9 mmol) was added dropwise to dry DMF (8.8 mL, 114.5 mmol) while maintaining the temperature below 25 °C using an ice bath. After complete addition, the mixture was stirred for 30 min at r.t. To this mixture was added **4** (400 mg, 0.618 mmol) in 80 mL dry DCE and the reaction was stirred for additional 5 h at 60 °C. After cooling to r.t., the mixture was slowly poured into a sat. aq. solution of $NaHCO_3$ (100 mL) under ice conditions, and further stirred for 60 min. Then, H_2O (20 mL) was added, and the resulting mixture was extracted with DCM (3 x 50 mL). The combined organic phases were dried over Na_2SO_4, filtered and solvents were concentrated under vacuum. The crude product was purified using automated flash chromatography reversed phase (H_2O:ACN + 0.05 % FA, gradient flow 5 % to 100 % ACN for 30 min) to afford the respective product **BDP** (110 mg, 26 %) as red-green, fluorescent solid. **^{1}H NMR** (500 MHz, $CDCl_3$) δ 10.05 (s, 2H), 7.16 (d, J = 8.5 Hz, 2H), 7.10 (d, J = 8.5 Hz, 2H), 4.22–4.19 (m, 2H), 3.94–3.90 (m, 2H), 3.77–3.57 (m, 20H), 3.36 (s, 3H), 2.86 (s, 6H), 1.76 (s, 6H). **^{13}C NMR** (126 MHz, $CDCl_3$) δ 185.54, 160.42, 160.14, 148.24, 147.41, 132.14, 128.59, 127.87, 125.40, 115.79, 71.81, 70.81, 70.48, 70.40, 69.51, 67.54, 58.92, 13.64, 12.21. **HRMS** calcd for $C_{34}H_{46}BF_2N_2O_9$ $[M + H]^+$: 675.32598, found 675.32837.

*Lysine Hydrazide (**Lys**).*

The synthesis of compound **2** was performed according to literature [37]. To a solution of L-Lysine methyl ester dihydrochloride (200 mg, 0.86 mmol) in anhydrous MeOH (4 mL) was added hydrazine hydrate (w % of N_2H_4 64–65 %) (0.25 mL, 6.86 mmol) and the reaction was stirred at r.t. for 24 h. After the completion of the synthesis, MeOH was removed under vacuum (60 °C , 20 mPa). Finally, 4 mL distilled H_2O is added to the product and freeze dried overnight to remove excess hydrazine hydrate. The product **Lys** (80 mg, 80 %) was obtained as a transparent oil. Care was taken to avoid exposure to moisture. **^{1}H NMR** (500 MHz, D_2O) δ 3.49 (t, J = 6.6 Hz, 1H), 3.03–2.97 (m, 2H), 1.74–1.65 (m, 4H), 1.44–1.32 (m, 2H).

Synthesis of BDP-Lys.

BODIPY-dialdehydes (BDP) and lysine hydrazide (Lys) monomers were dissolved in deuterated DMSO with 10 mM deuterated acetic acid (pH 3.0) to achieve 20 mM concentration. Then, they were mixed at 1:1 M ratio to yield a final concentration of 10 mM. The mixture was left reacting for 48 h at r.t. and excluded from light. The polymerization

completion was monitored by ^{1}H NMR at different time points, showing depletion of the aldehyde peak and successful polymerization (Fig. S7). The formed BDP-Lys were lyophilized without any washing step assuming complete consumption of the BDP monomers as indicated by the absence of aldehyde peaks. Another indication of successful polymerization is the change in color from light-red fluorescent to dark purple color with time.

2.3. Structure characterization of BDP-Lys

Size Exclusion Chromatography (SEC).

SEC was carried out determining the molar mass distributions ($Đ$), weight average molecular weight (M_w), number average molecular weight (M_n) employing a setup consisting of a 515 HPLC pump by Waters, a RI Waters 2410 and an UV Waters 2487 as the detectors and a PSS Gram column setup (30 Å, 2x 1000 Å) at 60 °C. DMF with 1 g/L LiBr was used as the eluent with a flow rate of 1 m/min and calibration were carried out using PEG standards from PSS.

Cryogenic Transmission Electron Microscopy (cryo-TEM).

Cryo-TEM images of the biodynamer were obtained using a JEM-2100 LaB_6 (JEOL, Akishima, Japan) microscope. A droplet (3 μL) of the molecular biodynamer solution (1 mg/ml, in a mixture of 10 % DMSO in H_2O) was placed on a S147-4 holey carbon film (Plano, Germany) and blotted to a thin liquid film for 2 s. Afterward the sample was plunged at T = 108 K into liquid ethane using a Gatan (Pleasanton, USA) CP3 cryo plunge system and transferred under liquid nitrogen to a Gatan 914 cryo-TEM holder operating at T = 100 K. Then cryo-TEM measurements were performed at an accelerating voltage of 200 kV at low-dose conditions.

Small-Angle Neutron Scattering (SANS).

Characterization of the BDP-Lys was carried out with SANS on D11 beamline at the Institut Laue-Langevin at Grenoble (ILL, France). By varying the wavelength of the incident beam and the sample to detector distance one can access the scattering vector $q = \frac{4\pi}{\lambda} sin\frac{\theta}{2}$ where θ is the angle between the direct and the scattered beam. Three sets of wavelength λ and sample-to-detector distance D were used : $\lambda = 11.5$ (Å), D = 17.6 (m); $\lambda = 6$ (Å), D = 17.6 (m); $\lambda = 6$ (Å), D = 5.6 (m) allowing measurements with q-ranges of $4.7 \times 10^{-4} \leq q$ (Å^{-1}) $\leq 1.4 \times 10^{-2}$, $3.7 \times 10^{-3} \leq q$ (Å^{-1}) ≤ 0.6, and $1.1 \times 10^{-2} \leq q$ (Å^{-1}) ≤ 0.7, respectively. Conversion to absolute intensity units (cm^{-1}) followed classical data reduction procedures that are corrections for empty cell, electronic background, detector response and normalization by the attenuated beam. The incoherent scattering leading to a plateau in the high-q region of the sample scattering curve is due to hydrogen atoms coming from the macromolecule and the solvent. Incoherent scattering masks structural correlations; therefore, it was substracted from the data. The high q data can be fitted by a Guinier expression for the form factor of the cross-section:

$$I(q) = \frac{A}{q} e^{-\frac{R_c^2 q^2}{2}} \quad (1)$$

Where $A = \varphi \Delta\rho^2 \pi a_c$, a_c is the section area of the filaments, R_c the radius of gyration of the cross section, φ the volume fraction of monomers and $\Delta\rho$ the difference in the scattering length density between the solvent and the scattering object.

The scattering intensity for a centosymmetric object is given by

$$I = \varphi V \Delta\rho^2 P(q) S(q) \quad (2)$$

Where

φ: volume fraction of repeating units.

V the volume of the scattering object, i.e. of the N repeating units (monomers) in a chain

$P(q)$: the form factor.

$S(q)$: the structure factor.

Small-Angle X-Ray Scattering (SAXS).

SAXS measurements were performed on the Xeuss 2.0 diffractometer at CEA-Saclay, at a wavelength λ of 1.54 Å. For the low scattering vector range a sample-to-detector distance of 2500 (mm) was used with collimating slits of 0.6 x 0.6 (mm) and 0.5 x 0.5 (mm), at the collimation distance of 1200 (mm). For the high-q range, the sample-to-detector distance was set at 540 (mm), the collimation slits dimensions were 1.2 x 1.2 and 0.8 x 0.8 (mm), and the collimation distance was 1200 (mm). The scattering wavevectors investigated were in the range of 4.4×10^{-3} (Å^{-1}) $\leq q \leq 1.1$ (Å^{-1}) and standard procedures were employed for reducing the data to absolute units (cm^{-1}).

For SANS the scattering length density is determined by $\rho = \frac{\Sigma n_i b_i}{m \times v / N_A}$ where n_i is number of atoms of the monomer or solvent, b_i the scattering length, N_A the Avogadro's number, m the molar mass of monomer or solvent, and v the specific volume of the repeating unit (or solvent molecule).

Since neutrons interact with the nuclei of atoms, the neutron scattering length b_i depends on the isotope. In contrast, for SAXS the electron cloud of the atom determines the propability for the scattering and so b_i is replaced by $Z_i \times r_e$ where Z_i is the atomic number of the ith atom and $r_e = 2.81 \times 10^{-13}$ (cm) is the electron radius. Scattering length densities ρ, the contrast terms $\Delta\rho$ calculated both for the whole BDP-Lys monomer unit and for the different parts of the dynamer as well as for the solvent are collected in Table S2 (Supporting Information).

2.4. Quenching of BDP-Lys fluorescence and absorbance

BDP and BDP-Lys were diluted in a solvent mixture of 1 % DMSO in H_2O containing 1 % polyvinyl alcohol (PVA) to achieve a final concentration of 25 μM. The fluorescence emission and absorbance scan before and after polymerization was measured using microplate reader (Infinite 200 PRO, Tecan Instruments, Männedorf, Switzerland), by taking 180 μL of the final solution into a black-96 well plate. For emission scan, the samples were excited at $\lambda = 470$ nm and highest emission for monomer/polymer was $\lambda = 520$ nm/ 550 nm (broad) respectively.

Based on preliminary experiments, we selected a 470 nm excitation wavelength for effective BDP monomer excitation and used it consistently to compare monomeric and polymeric BDP-Lys, highlighting its degradation and fluorescence enhancement.

2.5. Dequenching of BDP-Lys by pH-responsive degradation

To analyze pH-responsive fluorescence emission, BDP-Lys and BDP monomer were each diluted in a mixture of 1 % DMSO in the corresponding buffer solutions (10 mM containing 1 % PVA) to achieve a final concentration of 25 μM. The buffer solutions used included phosphate buffers at pH 3, 7.4, and 11, acetate buffer at pH 5, and carbonate buffer at pH 9. Fluorescence intensity was measured using the microplate reader, by taking 180 μL of the final solution into a black 96-well plate, with excitation at $\lambda = 470$ nm and emission at $\lambda = 520$ nm at various time intervals (0, 1, 3, 6, 9, 24, 48, 72, and 94 h) in each pH media.

The effect of pH on the absorbance of BDP-Lys and BDP monomer was carried out following the same procedure as the fluorescence measurements, with absorbance specifically measured at 502 nm. The experiment was independently performed twice, with triplicates.

2.6. Fluorescence monitoring of BDP with sodium ascorbate in pH 3

BDP monomers were diluted in a mixture of 1 % DMSO in the respective phosphate buffer (pH 3, 10 mM with 1 % PVA) with or without sodium ascorbate (E301), to achieve a final concentration of 25 μM. The first sample contained BDP diluted solely in the pH 3 buffer. The second sample included BDP diluted in pH 3 buffer containing 250 μM E301 (prepared by dissolving 0.5 mg of E301 in a 10 mL pH 3 buffer). In the final sample BDP was diluted in pH 3 buffer containing 20 mM E301

(prepared by dissolving 40 mg of E301 in a 10 mL pH 3 buffer). Fluorescence intensity was measured at various time intervals (0, 1, 3, 6, 9, 24, 48, 72, and 94 h) using a microplate reader. 180 μL of each solution was transferred into a black 96-well plate for measurements. The excitation and emission wavelengths were set at $\lambda = 470$ nm and $\lambda = 520$ nm, respectively. These measurements were used to observe the fluorescent behavior of the monomer in the presence and absence of E301. The experiment was performed twice, each with duplicates samples.

2.7. pH-responsive degradation of BDP-Lys

Dialysis was performed using a membrane with a molecular cut-off of 6 kDa. BDP-Lys was dissolved in DMSO: H_2O (1:1) at a concentration of 300 μg/mL and loaded into the membrane. The sealed dialysis membrane was then immersed in a beaker containing 100 mL of each respective buffer solutions (10 mM containing 1 % PVA of each phosphate buffer pH 3, pH 7.4 and acetate buffer pH 5). The dialysis was carried out at 37 °C with gentle stirring for 3 days. At various time points (0, 3, 6, 9, 24, 48, 72 h), 180 μL aliquots were withdrawn from the dialysate. The degraded amount of BDP-Lys was determined by measuring the absorbance at $\lambda = 502$ nm using the microplate reader. Calibration curves were done using BDP monomer. Dialysis experiments were conducted twice in triplicates.

2.8. Cytotoxicity assay

A549 cells were seeded into 96 well plates with 20 000 cells/well in RPMI medium supplemented with 10 % FCS. The plate was incubated until cells reached 95 % confluency with fresh medium added every 2 days. On the day of the experiment, the medium was removed. Then, the cells were washed twice with HBSS buffer and treated with the desired concentration of BDP-Lys (25, 50, 100, 200, and 400 μg/mL) and BDP monomer (31, 63, 125, 250, and 500 μg/mL) in HBSS. The dead control was 2 % TritonX-100 in HBSS, and the live control was HBSS. The cells were incubated at 150 rpm shaking at 37° C with 5 % CO_2. After 4 h, the treatment was removed, and the cells were washed once with HBSS. 100 μL HBSS + 10 μL PrestoBlue™ Cell Viability Reagent were added on the cells for 4 h while shaking. Fluorescence was measured by the plate reader at an excitation of 570 nm and an emission of 610 nm. % Viability was calculated as follows:

$$\%viability = \frac{Fl.ofsample - Fl.ofdeadcontrol}{Fl.oflivecontrol - Fl.ofdeadcontrol} * 100\%$$

2.9. Cellular uptake assay

To prepare our labeled BDP-Lys for cellular uptake studies, we began by preparing BDP-Lys as a 40 mM solution and Alexa Fluor 594 (AF594) as a 2 mM solution in DMSO. Subsequently, equal volumes of the two solutions were mixed to achieve the desired molar ratio: 20 mM product with 5 % dye incorporation. The mixture was allowed to stir for 24 h at r.t., shielded from light. Subsequent purification was performed by washing the sample with 0.01 % TEA using an Amicon Ultra filter, employing a centrifugation step at 5000 g for 10 min and repeating this wash process three times to eliminate all unbound AF594. Finally, the purified product was lyophilized and used as-is for further experiments.

A549 cells were seeded on a black 24-well plate with transparent bottom at a density of 100 000 cells/well for CLSM imaging. After 48 h incubation, cell medium was exchanged and further incubated until cells reached 90–95 % confluency. The cells were washed with HBSS buffer (x2) and then the desired labelled BDP-Lys-594 (500, 100, 50 and 10 μg/mL) in HBSS (500 μL) was added. After 4 h incubation at 37 °C, cells were washed again with HBSS (x2) and fixed using 4 % paraformaldehyde (PFA) (500 μL) for 30 min at r.t. After rinsing with HBSS (x2), cells nuclei were stained for 20 min with DAPI (Sigma; 0.5 μg/mL in HBSS). Cells were washed with HBSS and membrane was stained using Concanavlin A Alexa Fluor 633 Conjugate (Fisher Scientific; 5 μg/mL). After rinsing with HBSS, cells were analyzed by CLSM.

Confocal Laser Scanning Microscopy (CLSM): Images acquisition was performed using Fluotar VISIR 25x/0.95 water and the following settings were used: BD-Lys-594 fluorescent (excited at 561 nm, 2 % laser intensity) was detected between 590–610 nm. For DAPI and Concanavlin A, the emission filters were set between 410–466 nm (excited at 405 nm, 10 % laser intensity) and 650–776 nm (excited at 633 nm, 1 % laser intensity), respectively. Confocal z-stacks were recorded in a range of 50 μm and images were processed with the Leica Application Suite (LAS) X Software.

2.10. In-vitro BDP-Lys degradation

50,000 A549 cells were seeded in 250 μl RPMI medium supplemented with 10 % FCS in half of the wells of a 48-well plate (Ref 677180, Greiner Bio-One GmbH, Frickenhausen, Germany) and incubated for 24 h. Then, cells were washed twice with HBSS and 250 μl PBS was added to three wells containing cells and three empty wells. To these 6 wells, BDP-Lys was added at a concentration of 20 μg/well and cells were incubated at 37 °C in a 5 % CO_2 atmosphere. After 4 h, wells containing cells were washed twice with PBS and 250 μl PBS was added again. The 48-well plate was put inside a standard humidity cassette (large, Tecan Trading AG, Switzerland) containing 6 mL deionized H_2O in each reservoir and the cells were incubated at 37 °C and 5 % CO_2 in the Tecan SparkCyto (Tecan Trading AG, Switzerland) for 48 h. Cells were imaged at baseline (t = 0 h) and after 48 h using both brightfield and green fluorescence channels. Fluorescence images were captured with an LED intensity set to 80 % and an exposure time of 70 ms. Additionally, fluorescence intensity of all wells containing BDP-Lys was measured every 6 h using an excitation wavelength of 470 ± 15 nm and an emission wavelength of 520 ± 10 nm with 4 × 4 reads taken per well.

2.11. Estimating the degradation of polymer intracellularly vs time

20,000 A549 cells were seeded into 48-well plate. Cells were left to grow until 90 % confluency. Before t0 by 4 h, 20 μg/well of BDP and BDP-Lys were added into separate wells. Cell control wells were included for the background subtraction later and cells were incubated in a 37 °C with 5 % CO_2. At 0 h (after 4 h incubation), cells were washed and PBS was added, then fluorescence emission scan was measured between 500 and 700 nm, by exciting the samples at 470 nm using the microplate reader, with a manual gain of 80 at 0 h and 24 h.

The fluorescence signal (Fl_{total}) was subtracted from the average cell fluorescence (Fl_{cell}) to get the pure polymer or monomer fluorescence (pFl)

$$pFl = Fl_{total} - Fl_{cell}$$

Then the degree of polymerization or monomer portion (M Index) was estimated for the monomer and polymer at 0 h and 24 h via the ratio between fluorescence at 518 and 578 nm, using the following equation:

$$Mindex = \frac{pFl_{518nm}}{pFl_{578nm}}$$

Finally, degree of degradation was estimated via the following equation:

$$Degradation(\%) = \frac{Mindex_{polymerat24h} - Mindex_{polymerat0h}}{Mindex_{Monomerat24h} - Mindex_{polymeratoh}}$$

Two replicates were conducted, and standard deviation was calculated.

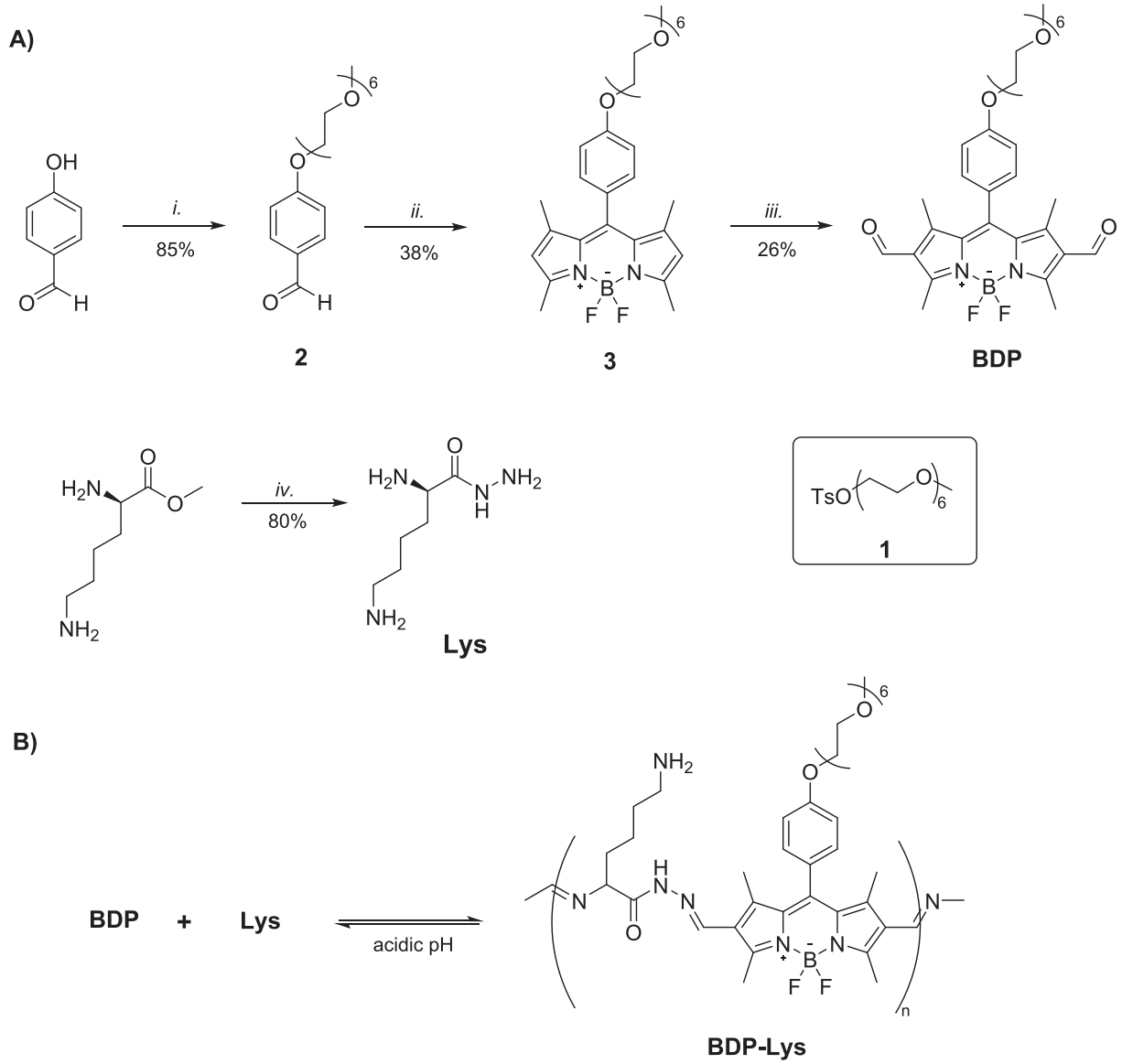

Scheme 1. (A) Synthesis of monomers BODIPY-dialdehydes (BDP) and lysine hydrazide (Lys). Reagents and conditions: i. 1, Cs_2CO_3, NaI, DMF, 12 h; ii. TFA, DDQ, TEA, $BF_3{\cdot}OEt_2$, DCM, 18 h; iii. (4) DMF, $POCl_3$, DCE, 50 °C 2 – 5h, reaction repeated twice to generate the di-aldehyde structure; iv. N_2H_4, MeOH, 24 h. (B) Hexaethylene glycol conjugated BDP and Lys polymerized reversibly into biodynamers by acylhydrazone and imine bond formation in acidic medium (pH 3.0).

3. Results & discussion

3.1. Synthesis of monomers

The corresponding monomers BDP and Lys were prepared as illustrated in Scheme 1A (detailed in Scheme S1). The synthesis began with 4-hydroxybenzaldehyde, which was converted to substituted aryl aldehyde **2**. BODIPY cores are usually constructed by the condensation reaction between a carbonyl group and a pyrrole followed by *in situ* complexation with boron trifluoride etherate ($BF_3{\cdot}Et_2O$) in the presence of a base [38]. Compound **3,** therefore, was obtained from reacting 2,4 dimethylpyrrole with aryl aldehyde **2**, followed by treatment of the reaction mixture with each $BF_3{\cdot}OEt_2$ and TEA. Subsequently, both formyl groups were introduced via a Vilsmeier-Haack reaction, in a two-step process, yielding the corresponding monomer BDP as a red fluorescent compound. The synthesis of the Lys monomer was achieved by treating L-Lysine methyl ester dihydrochloride with hydrazine hydrate in MeOH. The chemical structures of each monomer were characterized by ^{1}H NMR and ^{13}C NMR spectrometry (Figs. S1–S6).

3.2. Synthesis of BDP-Lys

We generated BDP-Lys biodynamer (BDP-Lys) using reversible C=N bond formation. It is a condensation reaction between aldehydes and primary amines or hydrazides, known as the Schiff-base reaction. Formed imines and acylhydrazones often exhibit rapid interconversion rates between formation and hydrolysis, particularly under acidic conditions [39]. The polycondensation of BDP and Lys monomers (Scheme 1B), following Carother's equation, was carried out at a 1:1 M ratio with a final concentration of 10 mM in a solvent mixture of DMSO and acetic acid. After 48 h at r.t., BDP-Lys polymerization was monitored by ^{1}H NMR spectroscopy (Fig. S7). Notably, during the reaction, the aldehyde C-H resonance at δ = 10.0 ppm was completely depleted after 48 h, indicating the consumption of BDP monomers through imine and acylhydrazone bond formation. These bond formations are evident around δ = 12.0 ppm. Extreme peak broadening in the aliphatic region is a typical feature of polymers, mainly caused by intramolecular interactions.

In the context of polymerization selectivity, α-position amines are known to be more reactive than ε-position amines and predominantly

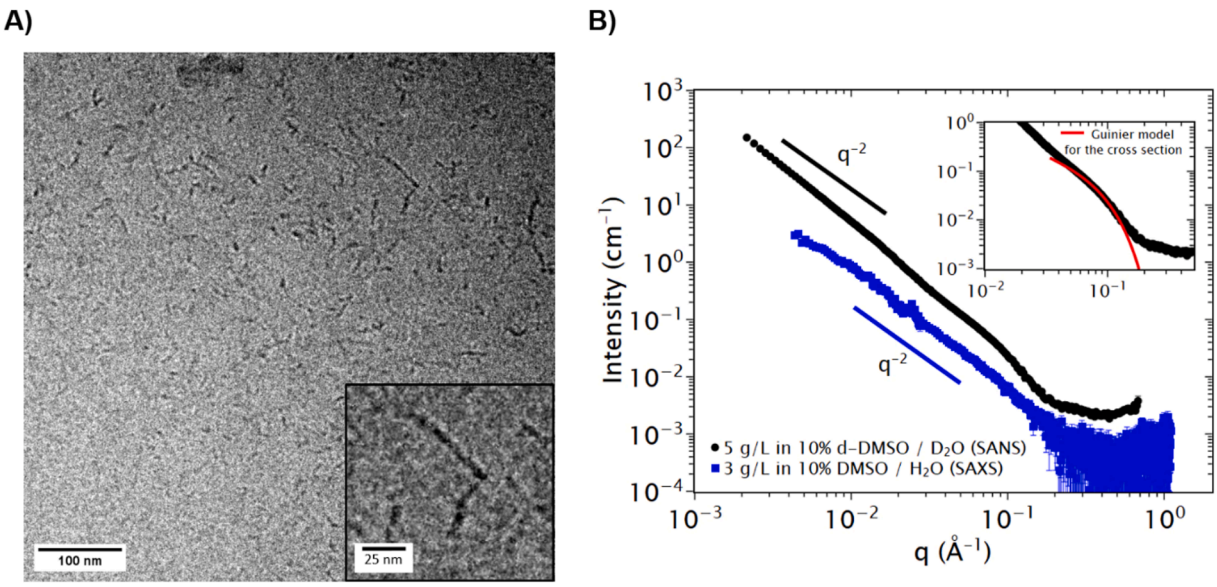

Fig. 1. (A) Cryo-TEM image of BDP-Lys at a concentration of 1 g/L in a mixture of 10 % DMSO in H_2O. (B) Scattering patterns for BDP-Lys: SANS measurements of solution of BDP-Lys at a concentration of 5 g/L in a mixture of 10 % d-DMSO in D_2O (black squares) and SAXS measurements at a concentration of 3 g/L in a mixture of 10 % DMSO in H_2O (blue squares). For SAXS, the scattering intensity was measured at two configurations, whereas for SANS it was measured at three different configurations of wavelength λ and sample-to-detector distance D (11.5 (Å) – 17.6 (m), 6 (Å) – 17.6 (m), 6 (Å) – 5.6 (m)), allowing for a wider q-range. Inset: The high-q data were fitted using a Guinier model for the cross section (red line) giving a characteristic radius of gyration R_c of 15 Å for the cross section, and a cross-sectional area a_c of 365 Å^2. (For interpretation of the references to color in this figure legend, the reader is referred to the web version of this article.)

participate in biodynamer polymerization. This higher reactivity of α-amines is attributed to their greater nucleophilicity, as the adjacent carbonyl group enhances electron density and stabilizes the developing positive charge. Furthermore, cation–π and electrostatic interactions restrict the accessibility of ε-amines, which are more susceptible to be protonated than α-amines, thereby favoring α-amines as the preferred sites for imine bond formation [40,41].

3.3. Molecular weight estimation of BDP-Lys

The resulting polymers were injected into SEC to confirm the polymerization. The measurements of BDP-Lys were carried out in DMF with PEG standard at a concentration of 0.6 g/L. A molar mass of approximately $M_w = 10\,000$ g/mol, with a dispersity ($Đ$) value of 10.4 has been observed after the polymerization (Figs. S8), suggesting a broad molecular-weight distribution.

This broad dispersity can be attributed to the specific polymerization conditions, the underlying mechanisms and the fact that the polymer was analyzed without purification to allow a direct comparison with the previously reported biodynamer. In the case of the previously CA-based biodynamer, the hydrophobic CA core gained water solubility due to the attached hydrophilic HG chains, allowing polymerization in an aqueous environment following a nucleation-elongation (N-E) mechanism [40–42]. A key feature of N-E polymerization is the formation of a critical polymer chain length, after which elongation becomes more favorable than initiating new chains. This process was driven by the enhanced stability of CA-based biodynamer, resulting from hydrophobic interactions and $\pi - \pi$ stacking, and folding of CA core units. Meanwhile, the hydrophilic HG chains extended into the solvent, promoting a more stable and controlled nucleation-elongation process [40]. In contrast, BDP-Lys polymerization was conducted in DMSO due to the poor BDP solubility in water, even in the presence of the hydrophilic HG chain. DMSO, being a polar aprotic solvent, ensured the solubility of both monomers, facilitating polymerization. However, these conditions weaken the N-E mechanism by decreased hydrophobic interaction between the monomers, and accelerate the reaction kinetics, which was observed by the immediate color change from red to purple upon lysine addition. This fast reaction rate is characteristic of an uncontrolled step-growth condensation polymerization and uncontrolled nucleation events, which, according to Carothers' theory, inherently leads to broad molecular weight distributions as observed in SEC measurements. To obtain a refined BDP-Lys biodynamer, further optimization of polymerization conditions or modification of monomer structures to enhance their water solubility may be necessary.

3.4. Structure analysis of BDP-Lys

To provide complementary information on the structure of the BDP-Lys, a certain set of experimental techniques has been found to be useful in the context of biodynamers, including cryogenic transmission electron microscopy (cryo-TEM) [43], small-angle neutron (SANS) [44], and X-ray (SAXS) scattering [45]. Fig. 1A shows a micrograph of a vitrified solution about 200 − 300 nm thick at $c = 1$ g/L (in a mixture of 10 % DMSO in H_2O). The image shows polydisperse rod-like filaments of various lengths (8–100 nm) with random orientations relative to the plane of observation and with a high optical density cross-section suggesting a local molecular packing [41]. The inset displays a magnified image of a long filament larger than 60 nm. A common feature is that filaments are rigid over long lengths. They also appear to exhibit regular sequences of alternating gray and black regions of higher electronic contrast along the main axis of the filaments. The inset of Fig. 1A allows for the measurement of a cross-sectional diameter of $D_{c\text{-TEM}} = 4$ nm. This dimension is larger than the monomer unit diameter ($D_{mon} < 11$ Å (calculated by Avogadro excluding HG)), indicating a well-defined local organization and molecular packing inside the assemblies, as previously observed for similar biodynamers [30].

To obtain more precise insights on the local structure and conformation of the assemblies, we employed SANS and SAXS, complementary techniques well-suited for probing structural parameters and molecular organization over the range of 1–30 nm.

A typical SANS scattering pattern representing the variation of the scattered intensity with the magnitude of the scattering wave-vector q can be visualized in Fig. 1B for BDP-Lys at the concentration $c = 5$ g/L. The absence of a Guinier plateau, associated with objects of finite mass

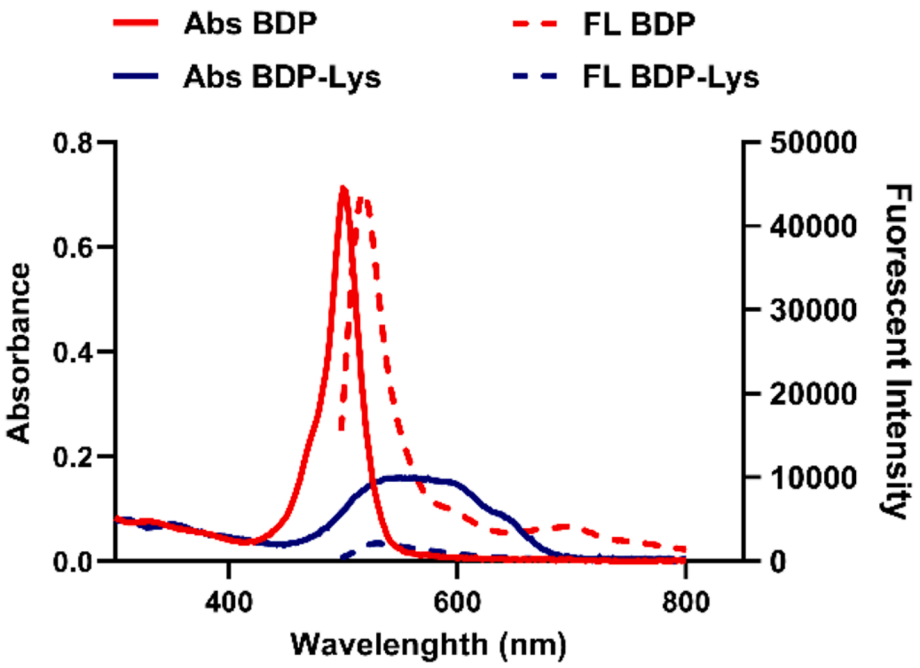

Fig. 2. Optical changes by molecular biodynamer formation showing absorbance (straight line) and fluorescence (dotted line) at a concentration of 25 μM in a mixture of 1 % DMSO in H_2O, when excited at $\lambda = 470$ nm. Fluorescent quenching of BDP monomer and the peak shifted from $\lambda = 520$ nm (dotted red line) to a broad signal of $\lambda = 530 - 560$ nm (dotted blue line). Absorbance broadness and shift of BDP monomer peak after polymerization (blue line). (For interpretation of the references to color in this figure legend, the reader is referred to the web version of this article.)

and size, in the low-q region indicates that the size of the self-assemblies is larger than 30 nm. Instead, we observe an extended regime which can be described by a power law with characteristic exponent equal to − 2, as for Gaussian chains or for a planar 2D local organization or stacking. This q^{-2} regime is followed at higher q, i.e., larger than 0.06 $Å^{-1}$, by an exponential decay associated with the cross-sectional dimension of the filaments.

The high q data can be fitted by a Guinier expression for the form factor of the cross-section (Equation (1), see materials and methods), and the obtained parameters are collected in Table S1.

We found a value of 1.5 nm for the cross-sectional radius of gyration, R_c, corresponding to a diameter of about $D_{c\text{-SANS}} = 3$ nm, a value in good agreement with the section found from the cryo-TEM analysis ($D_{c\text{-TEM}} =$ 4 nm). The value of R_c is greater than $R_c > \sqrt{\frac{a_c}{\pi}}$, which suggests that the section of the filaments assumed to be circular is not full. At first sight, the q^{-2} regime could be associated with the random distribution of monomers as in a Gaussian wormlike chain. However, in this case, we would expect to observe a q^{-1} regime at larger scattering wavevectors q associated with the rigid behavior of the chain or filaments for distances smaller than the persistence length L_p, which is not the case. Another possibility is that the local organization of the filaments is planar, as is the case for helical or twisted ribbons. This could explain the rather large cross-sectional dimensions combined with a relatively small value of the cross-sectional area a_c. This also explains the regular alternations of contrast along the filaments observed in the cryo-TEM images. It should be noted that the small deviation from the observed q^{-2} behavior in the very low-q range could arise from the roughness of the 2D interface related to the hydrophilic side chains of the monomers or from the branching and/or aggregation of the filaments at larger scales, as observed by cryo-TEM.

More insight into the molecular packing and the hypothetical local 2D organization can be obtained using SAXS, a technique much more sensitive to the electronically dense parts of molecules, such as the aromatic groups of the hydrophobic core of the BDP. As a result, the contrast term $\Delta\rho$ for the hydrophobic aromatic core of the dynamer is much larger than that of the hexaethylene glycol chains (Table S2) and the SAXS signal will be dominated by the aromatic core, while the side chains and lysine will be invisible. By contrast, SANS is sensitive to the overall scattering objects. The scattering profile of SAXS displayed in Fig. 1B exhibits a clear extended q^{-2} power law, suggesting that the 2D local organization arises from the packing of the aromatic components. A rather weak bending is observed at small q, which, if real, could be associated with objects of finite size and mass. In this case, one could envisage a structure that would result from the self-association of small ellipsoids in the form of filaments. This model would explain why the SEC measurement (performed at lower concentrations) gives such small masses (mass of elementary ellipsoids) and why the filaments are so polydisperse.

3.5. Quenching of BDP-Lys fluorescence and absorbance

After confirming the structure of the prepared BDP-Lys through various characterization techniques, its fluorescence properties, arising from these structural features, were subsequently investigated. As previously discussed, BODIPY is a well-known fluorescent dye used in biological applications due to its high fluorescence quantum yield, independence of pH, and excellent photostability. However, it is also well known for aggregation-induced quenching (AIQ) by H-type (face-to-face) aggregation [46,47], which can occur during the polymerization, and can be strategically leveraged in biomedical applications [48]. Given the molecular packing of the hydrophobic core observed in SANS and SAXS, we expected that polymerization of BPD-Lys would lead to fluorescence quenching. It is important to note that the quenching arises from aggregation of BDP units within a single polymer chain, rather than from the aggregation of multiple BDP-Lys polymers into nanostructures, as each nanorod corresponds to a single polymer molecule, as shown in the cryoTEM.

At a concentration of 25 μM, BDP monomer exhibited sharp fluorescence emission and absorbance at $\lambda_{em} = 520$ nm and $\lambda_{abs} = 502$ nm, respectively. In contrast, after polymerization into the BDP-Lys form, significant changes were observed in both the absorption and fluorescence spectra (Fig. 2). The most notable change was a substantial

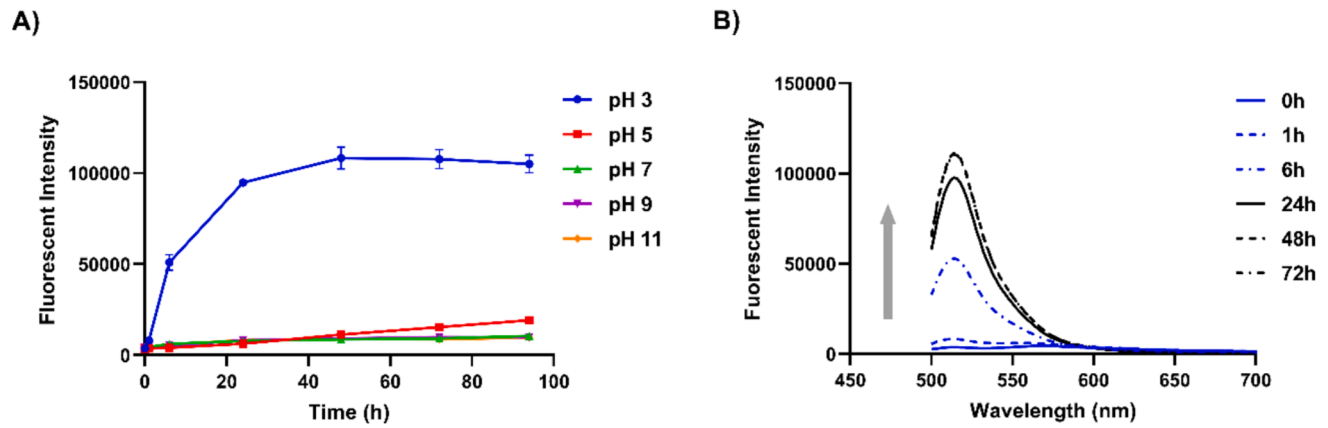

Fig. 3. Ph-responsive optical changes of bdp-lys: (a) fluorescence emission recovery of bdp monomer at $\lambda_{em} = 520$ nm in different pH at different time points. Errors bars were obtained from duplicated experiments (N = 2 and n = 6) (B) Emission shifts at pH 3 as a function of time. Broad peak shift from around $\lambda_{em} = 550–580$ nm to a sharp peak at $\lambda_{em} = 520$ nm. The concentration of BDP-Lys is set to 25 μM and 10 mM buffer solutions (pH 3–11) were used.

decrease in intensity along with considerable broadening of the peaks. This is interpreted as the result of AIQ caused by the reduced intermolecular distance between BDP units upon polymerization, which affected both absorption and emission. A closer examination of the absorption peak revealed the peak maximum redshift as a result of polymerization. This shift is also attributed to changes in the electronic environment arising from intermolecular interactions between BDP moieties. On the other hand, the emission spectrum showed negligible wavelength shift, likely due to the dominant influence of a small amount of unreacted BDP monomers or low-molecular-weight oligomers (e.g., dimers or trimers), which still emit strongly near the monomeric emission wavelength.

In addition to the AIQ of BODIPY, another possible explanation for these changes is the introduction of a C=N bond to the BODIPY core, which facilitates photoinduced electron transfer (PET) processes. The acylhydrazone and imine bonds formed act as an electron-withdrawing group (EWG), promoting PET from the BODIPY core to the C=N moiety and leading to fluorescence and absorbance depletion. These observations align with previous reports [49,50], where C=N bonds caused a fluorescence turn-off of the BODIPY probe with the potential of re-inducing a turn-on by the removal of the reversible C=N moiety. Therefore, the formation of C=N bonds and polymerization-induced aggregation have a big influence on the photophysical properties of BODIPY, in particular leading to quenching of both fluorescence and absorbance.

3.6. Dequenching of BDP-Lys by pH

We anticipated that the polymerization-induced quenching of BODIPY could be reversed through acid-triggered degradation of the biodynamer, as BDP-Lys exhibits dynamic reversible behavior under acidic conditions due to the acylhydrazone and imine bonds in the backbone. Therefore, we evaluated the pH effect on the optical properties of the biodynamer. BDP-Lys was incubated in different buffer solutions (10 mM, pH 3–11) for 96 h at r.t., and the emissions were measured at different time intervals. As shown in Fig. 3A, the fluorescence emission remained stable in neutral (pH 7.4) and basic environments (pH 9 and 11) throughout the entire incubation period. However, a significant increase in fluorescence was observed at pH 3, with a 14-fold increase after 72 h, compared to the other pH conditions. Additionally, within the first hour of incubation at pH 3, the emission spectrum of BDP-Lys was broadened. Over the next 6 h, the broad peak gradually shifted to a single narrow emission at $\lambda = 520$ nm, corresponding to λ_{max} of the BDP monomer (Fig. 3B). Only protonation by acid alone is unlikely to counteract the AIQ effect and restore fluorescence. We, thus, believe that this emission increase and shift under acidic conditions result from the reversal of the previously described quenching effect, driven by the pH-responsive DCB in BDP-Lys and their subsequent hydrolysis into monomers e.g. degradation, indicating that BDP-Lys might be a useful tool for tracking polymer degradation under acidic conditions.

3.7. pH-Dependent fluorescence of BDP

Assuming that monomer release is responsible for the increase in fluorescence intensity, we also evaluated the possibility of acid-dependent fluorescence changes of the released monomer before

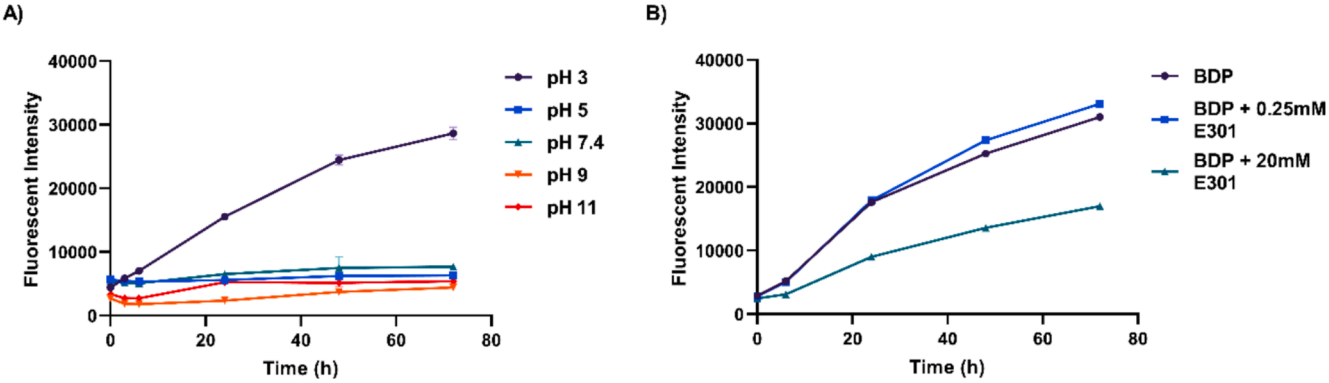

Fig. 4. Fluorescent emission spectra of (A) BDP monomer in different pH medium and various time points. (B) BDP monomer incubated at pH 3 in the presence of E301 (0.25 and 20 mM), highlighting the impact of the antioxidant on the stability and emission properties of the monomer under acidic pH.

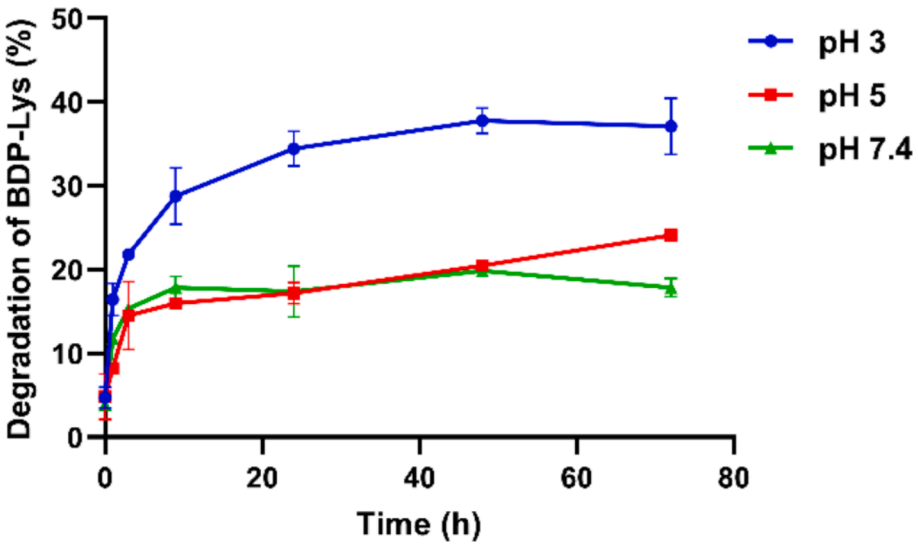

Fig. 5. Acid-responsive degradation of BDP-Lys at 37 °C (300 μg/mL) in phosphate buffer (pH 3 and pH 7.4, 10 mM) acetate buffer (pH 5, 10 mM). Errors bars were obtained from duplicated experiments (N = 2 and n = 3).

investigating relation of fluorescence increase and polymer degradation. While investigating the pH effect on BDP, a significant fluorescence emission increase was observed. The fluorescence emission of the BDP monomer increased over time after incubation at pH 3 but remained stable in other media (pH 5–11, Fig. 4A).

This fluorescence change is attributed to the presence of the aldehyde groups, which are prone to protonation and oxidation to carboxylic acid in acidic pH conditions [51,52]. As EWG, aldehydes can increase the electron deficiency of the BODIPY core, facilitating intramolecular charge transfer and PET, both critical for changing fluorescence. Therefore, the oxidation of the aldehyde group has a possibility of an enhancement in fluorescence. Additionally, the oxidation to carboxylic acid group may improve the solubility of BDP, as the hydroxyl and carbonyl group increase polarity, which can further contribute to fluorescence enhancement. Similar behavior has been reported in various studies, where certain BODIPY derivatives show marked fluorescence enhancement at acidic pH due to the protonation of respective EWG moieties [53–56] or cleavage of ester group to carboxylic acid [57]. Given that the fluorescence of BDP increase at pH 3 required almost 24 h, we speculate here that protonation followed by oxidation restored fluorescence intensity.

To further support this hypothesis, we incubated BDP at pH 3 with the presence of antioxidant, sodium ascorbate (E301), and analyzed the effect in fluorescence under conditions that restrict oxidation at low pH. As shown in Fig. 4B, the addition of 20 mM E301 suppressed the increase in fluorescence emission, supporting that the oxidation was involved in the fluorescence enhancement under acidic conditions. Therefore, not only low pH conditions, such as pH 3, but also reactive oxygen species (ROS)- and enzyme-mediated oxidation, could potentially enhance the fluorescence intensity of the monomeric BDP. For example, aldehyde dehydrogenases (ALDH) are responsible for the oxidation of aldehydes to carboxylic acids, and protect living organisms against oxidative stress [58,59]. Thus, we expect that the fluorescence increase of the released monomers after BDP-Lys degradation will be advantageous feature of the system. Although investigation into enzymatic oxidation of the monomer in biological systems was not feasible with the current monomer due to the limited solubility, additional investigations with modified versions of the BDP, and their pathways will further prove this hypothesis.

3.8. pH-responsive degradation of BDP-Lys

Next, we monitored BDP-Lys degradation, which might be associated with the fluorescence increase. Given that the fluorescence of BDP monomer is pH-dependent, we first confirmed its absorbance stability across different pH levels (pH 3, 5 and 7.4) to ensure accurate data. The absorbance of the BDP monomer remained stable and independent of pH changes (Fig. S9). Therefore, the degradation degree of BDP-Lys was determined by measuring the absorbance at 502 nm. Approximately 37 % of BDP-Lys degraded into monomers and oligomers smaller than 6 kDa at pH 3 within 72 h. In contrast, about 15 % of BDP-Lys degraded in a buffer at pH 7.4 due to the limited dynamicity of the DCB (Fig. 5). This degradation under acidic conditions (phosphate buffer, pH 3), recovered BODIPY fluorescence by 14-fold during a 72-h incubation at 37 °C. Considering the correlation between its degradation and the fluorescence increase, we can conclude that, at acidic pH, biodynamers start to shorten and fluorescence increases over time due to the polymer degradation with dynamic nature, followed by oxidation of the BDP.

The high stability of BDP-Lys under acidic conditions, along with its limited degradation, is surprising given the inherent reactivity of imine and acylhydrazone bonds in the polymer backbone. The DCB, which was used in this polymerization process, is known to be unstable in aqueous media, and its application in polymer backbones has been very limited [60,61]. However, our previous work demonstrated that non-covalent bonds within the polymer, hydrophobic interactions and π-π stacking, stabilize the DCB, leading to enhanced polymerization efficiency and stability in aqueous media. For example, the CA-Lys biodynamer benefits from π-π stacking and hydrophobic interactions from the CA group along with cation-π stacking from the Lys residue [27,30,40]. This resulted in significantly higher polymerization efficiency, with a degree of polymerization (DP) reaching 100, compared to biodynamers without the CA group [30,42]. Moreover, in the case of CA-Lys, 60 % degradation was observed over 72 h at pH 5.0 [62].

For BDP-Lys, these stabilizing effects by non-covalent bonds were further enhanced, requiring additional conditions to make the DCB irreversible. In fact, BODIPY has a strong tendency for stacking, resulting in strengthening non-covalent bonds and significant quenching. Additionally, its limited solubility in aqueous solutions necessitated the use of DMSO as a solvent for polymerization, unlike CA-Lys. The increased hydrophobicity and enhanced π-π stacking likely shifted the equilibrium of DCB further toward bonding, making the polymer more stable to degradation in aqueous media. Consequently, although a mild

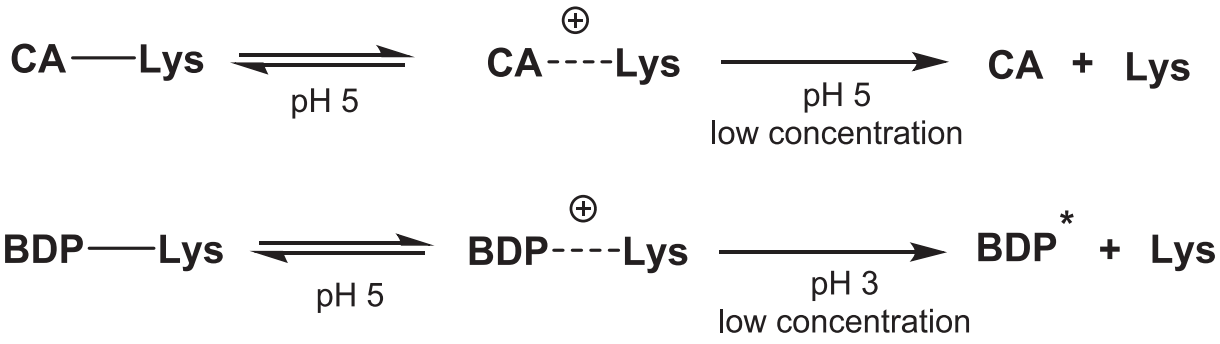

Scheme 2. Mechanism of both biodynamers CA-Lys and BDP-Lys: In CA-Lys, pH 5 with low concentration promotes degradation to monomers and irreversible DCB cleavage. In BDP-Lys, mild acidic conditions initiate DCB cleavage and degradation, while higher acidity (e.g. pH 3) triggers oxidation of BDP aldehyde to BDP*, making the DCB irreversible and enhancing fluorescence.

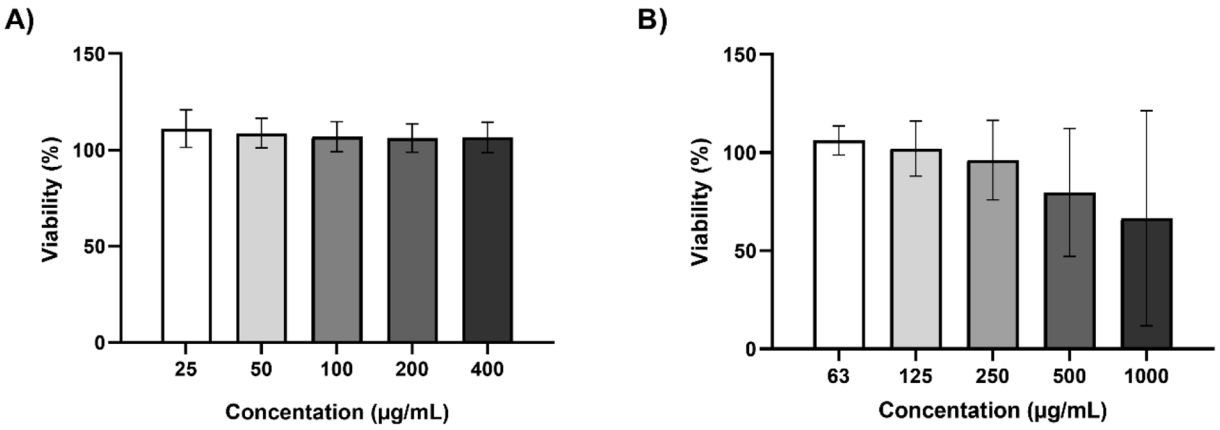

Fig. 6. Cell (A549) viability of BDP-Lys biodynamer (A) and BDP monomer (B). Viability was determined by Presto blue assay using Triton-X (2 %) as a positive control, after 4 h incubation with the respective samples at 37 °C. Errors bars were obtained from duplicate experiments (N = 2 and n = 3). (For interpretation of the references to color in this figure legend, the reader is referred to the web version of this article.)

acidic condition may be sufficient to trigger the cleavage of DCB within BDP-Lys, the bond can be later reversibly recovered under the mild acidic conditions. Thus, higher acidity concentration was necessary to promote the gradual oxidation of BDP's aldehyde groups, which caused DCB cleavage and irreversible polymer degradation (Scheme 2). This oxidation can occur not only at low pH but also by oxidants or intracellular oxidases such as ALDH as mentioned earlier. Therefore, we hypothesized that the increase in fluorescence intensity due to polymer degradation, similar to that observed at pH 3, could be achieved through the induction of degradation under intracellular mild acidic conditions and the inhibition of reversible reactions by intracellular oxidases.

3.9. Cell viability of BDP-Lys and their degradation products

Therefore, to examine the degradation of BDP-Lys within cells, its cytotoxicity was first confirmed. Cell viability of our biodynamer was conducted in the mammalian cell line A549, using Presto Blue as an indicator. The results in Fig. 6A show no significant toxicity of BDP-Lys across the tested concentration range, confirming its biocompatibility and safety for potential biomedical applications. In contrast, the BDP monomer (Fig. 6B), evaluated here as polymer degradation product, lowered cell viability to < 80 % at higher concentrations than 500 µg/mL. This toxicity may be due to dialdehyde groups within the molecule,

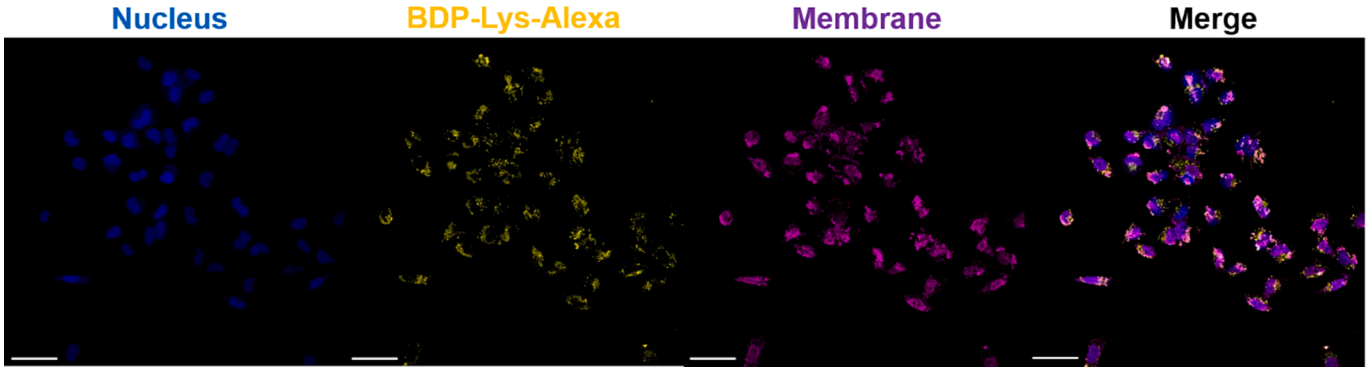

Fig. 7. Confocal laser scanning microscopy visualization of the A549 cellular uptake after incubation with BDP-Lys-Alexa for 4 h. DAPI-stained cell nuclei (blue), Concanavlin A Alexa Fluor™633 stained cytoskeleton (purple), and dynamer labeled BDP-Lys-Alexa (yellow). Scale bar is 50 µm.

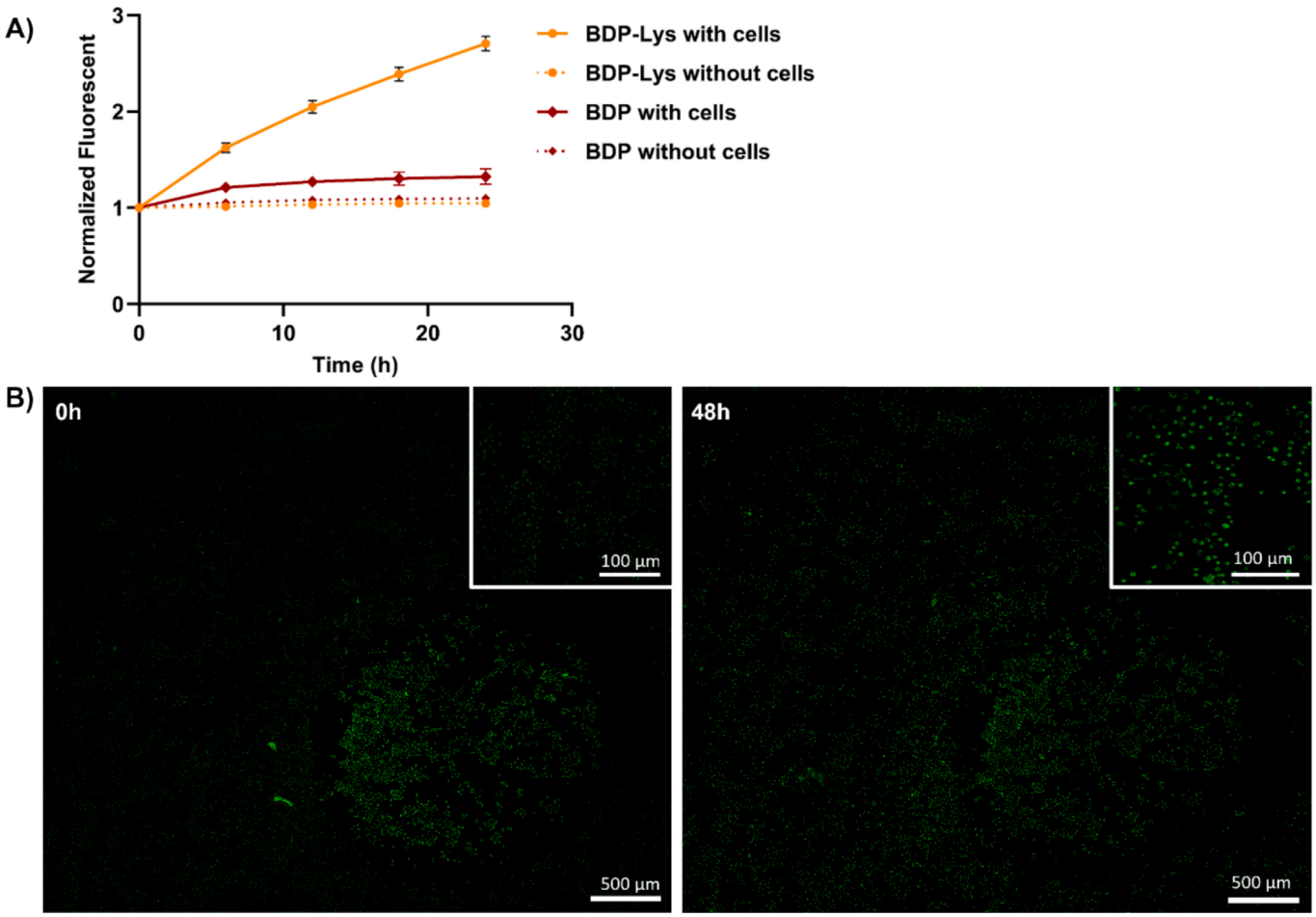

Fig. 8. Fluorescence intensity of BDP and BDP-Lys with and without A549 cells for 24 h. A) Normalized fluorescence intensity over time for BDP-Lys incubated with A549 cells and BDP-Lys without cells as control. B) Fluorescence plate-reader images of BDP-Lys incubated with A549 cells at 0 h (left) and 48 h (right).

consistent with results from previously investigated CA-Lys.

Moreover, Lysine hydrazide, another expected degradation product, was evaluated for cytotoxicity in earlier work and was found to reduce cell viability to below 80 % at a concentration of 250 µg/mL [63]. These results suggest that while the polymer itself is non-toxic, some degradation products exhibit concentration-dependent cytotoxicity, highlighting the importance of monitoring degradation behavior/rate for safe biomedical use.

3.10. Intracellular degradation of BDP-Lys

Before monitoring polymer intracellular degradation, we first assessed whether BDP-Lys could be efficiently taken up by cells. Due to the quenching of BODIPY intrinsic fluorescence in BDP-Lys, Alexa Fluor 594 dye was conjugated on the Lys side chain via amine-NHS ester reaction to monitor its cellular uptake. BDP-Lys-Alexa was incubated with A549 cells for 4 h at 37 °C. After incubation, cells were washed and stained with DAPI for the nucleus (blue) and Concanavalin Alexa Fluor 633 for the membrane (purple) to visualize intracellular structures using the confocal microscope. As shown in Fig. 7, there was a strong overlap between BDP-Lys-Alexa and the cytoplasmic region of the cells, confirming their high possibility of cellular uptake.

Following the confirmation of efficient cellular uptake, we aimed to evaluate polymer degradation and determine whether fluorescence recovery could be observed upon degradation of BDP-Lys within the cells. Thus, A549 cells were incubated with either BDP-Lys or BDP monomer (20 µg/well). After 4 h, cells were washed to remove any non-internalized materials that had not been taken up by the cells and then further incubated for 24 h.

Although the intracellular environment does not reach the highly acidic pH 3 used in our cuvette experiments, a significant increase in fluorescence intensity, approximately threefold, was observed for BDP-Lys after 24 h (Fig. 8). This clearly indicates that polymer degradation and subsequent BDP fluorescence recovery occur within cells. The observed fluorescence enhancement can be attributed to intracellular oxidative agents, such as ROS and ALDH, which facilitate the oxidation of aldehyde groups and irreversible cleavage of DCBs. Thus, these biological factors combined with mildly cellular acidic conditions promote polymer degradation and enable fluorescence activation under physiologically relevant conditions.

In contrast, only a slight fluorescence enhancement was observed when cells were treated with BDP monomers. This is likely due to its inherent hydrophobicity and poor aqueous solubility, which limit cellular uptake and lead to loss of unbound monomer during the washing steps. Importantly, the control sample without cells showed no changes in fluorescence, which is expected, since as previously demonstrated, biodynamers are stable in neutral conditions. This confirms that the fluorescence increase observed in the presence of cells is due to polymer degradation and subsequent BDP oxidation.

Moreover, this fluorescence increases within the cells allowed us to estimate the degradation rate of the BDP-Lys. The intracellular degradation kinetics was estimated using the characteristic fluorescence emission scan pattern, which was found to be different for BDP-Lys and its monomer, BDP (Fig. 2). The amount of released monomers from the BDP incubated in the cells was determined using fluorescence pattern of degrading BDP-Lys relative to the pure monomer pattern which was

considered as standard. Resultingly, BDP-Lys was degraded by about 17.07 ± 2.23 % in the first 24 h, reflecting specific rate constant (k) of 0.007 h^{-1}, assuming first-order degradation kinetics (see materials and methods for further details). Note that this is the maximum degradation rate, considering that fluorescence intensity also increases by the hour in cells.

4. Conclusions

In summary, our study detailed the design and synthesis of a novel biodynamer composed of BODIPY-dialdehyde (BDP) and lysine hydrazide (Lys), highlighting its dynamic nature in response to pH changes. By using ^{1}H NMR spectroscopy, cryo-TEM, SEC, SANS and SAXS, we characterized the polymerization and structure of the resulting BDP-Lys. We evaluated its optical properties, noting that fluorescence is quenched in polymeric form which is the case in neutral conditions. Under acidic conditions, however, as in certain intracellular compartments (e.g. lysosome), biodynamer fluorescence is de-quenched as a consequence of polymer degradation and subsequent oxidation of the released monomer. The *in vitro* studies highlight the cellular internalization of BDP-Lys leading to polymer degradation and successful fluorescence recovery within mammalian cells. Overall, BDP-Lys biodynamer provides a promising starting point for further investigation of polymer degradation and fate within biological systems. Considering the possibility to modify the amino acid monomer composition, BDP-based biodynamers offer great potential for both biomedical and drug delivery applications.

Funding

This research did not receive any specific grant from funding agencies in the public, commercial, or not-for-profit sectors.

Declaration of competing interest

The authors declare that they have no known competing financial interests or personal relationships that could have appeared to influence the work reported in this paper.

Acknowledgements

The authors would like to thank, Blandine Boßmann from Polymer Chemistry, Saarland University for help with SEC measurements.

Appendix A. Supplementary data

Supplementary data to this article can be found online at https://doi.org/10.1016/j.matdes.2025.114240.

References

[1] A. Zielińska, F. Carreiró, A.M. Oliveira, A. Neves, B. Pires, D.N. Venkatesh, A. Durazzo, M. Lucarini, P. Eder, A.M. Silva, A. Santini, E.B. Souto, Polymeric Nanoparticles: production, Characterization, Toxicology and Ecotoxicology, Molecules 25 (2020), https://doi.org/10.3390/molecules25163731.
[2] N. Kamaly, B. Yameen, J. Wu, O.C. Farokhzad, Degradable Controlled-Release Polymers and Polymeric Nanoparticles: Mechanisms of Controlling Drug Release, Chem. Rev. 116 (2016) 2602–2663, https://doi.org/10.1021/acs.chemrev.5b00346.
[3] R. De, M.K. Mahata, K.-T. Kim, Structure-Based Varieties of Polymeric Nanocarriers and Influences of their Physicochemical Properties on Drug delivery Profiles, Adv. Sci. 9 (2022) 2105373, https://doi.org/10.1002/advs.202105373.
[4] M. Redrado, Z. Xiao, K. Upitak, B.-T. Doan, C.M. Thomas, G. Gasser, Applications of Biodegradable Polymers in the Encapsulation of Anticancer Metal Complexes, Adv. Funct. Mater. 34 (2024) 2401950, https://doi.org/10.1002/adfm.202401950.
[5] R. Duncan, M.J. Vicent, Polymer therapeutics-prospects for 21st century: the end of the beginning, Adv. Drug Deliv. Rev. 65 (2013) 60–70, https://doi.org/10.1016/j.addr.2012.08.012.
[6] S. Parveen, R. Misra, S.K. Sahoo, Nanoparticles: a boon to drug delivery, therapeutics, diagnostics and imaging, Nanomedicine 8 (2012) 147–166, https://doi.org/10.1016/j.nano.2011.05.016.
[7] S. Roussel, P. Grenier, V. Chénard, N. Bertrand, Dual-Labelled Nanoparticles Inform on the Stability of Fluorescent Labels In Vivo, Pharmaceutics 15 (2023), https://doi.org/10.3390/pharmaceutics15030769.
[8] A.S. Klymchenko, F. Liu, M. Collot, N. Anton, Dye-Loaded Nanoemulsions: Biomimetic Fluorescent Nanocarriers for Bioimaging and Nanomedicine, Adv. Healthcare Mater. 10 (2021) e2001289, https://doi.org/10.1002/adhm.202001289.
[9] S. Bou, A.S. Klymchenko, M. Collot, Fluorescent labeling of biocompatible block copolymers: synthetic strategies and applications in bioimaging, Mater. Adv. 2 (2021) 3213–3233, https://doi.org/10.1039/d1ma00110h.
[10] V. Zhukova, N. Osipova, A. Semyonkin, J. Malinovskaya, P. Melnikov, M. Valikhov, Y. Porozov, Y. Solovev, P. Kuliaev, E. Zhang, B.A. Sabel, V. Chekhonin, M. Abakumov, A. Majouga, J. Kreuter, P. Henrich-Noack, S. Gelperina, O. Maksimenko, Fluorescently Labeled PLGA Nanoparticles for Visualization In Vitro and In Vivo: the Importance of Dye Properties, Pharmaceutics 13 (2021), https://doi.org/10.3390/pharmaceutics13081145.
[11] S. Snipstad, S. Hak, H. Baghirov, E. Sulheim, Ý. Mørch, S. Lélu, E. von Haartman, M. Bäck, K.P.R. Nilsson, A.S. Klymchenko, C. de Lange Davies, A.K.O. Åslund, Labeling nanoparticles: Dye leakage and altered cellular uptake, Cytometry A 91 (2017) 760–766, https://doi.org/10.1002/cyto.a.22853.
[12] A. Reisch, A.S. Klymchenko, Fluorescent Polymer Nanoparticles based on Dyes: seeking Brighter Tools for Bioimaging, Small 12 (2016) 1968–1992, https://doi.org/10.1002/smll.201503396.
[13] P. Álamo, V. Pallarès, M.V. Céspedes, A. Falgàs, J.M. Sanchez, N. Serna, L. Sánchez-García, E. Voltà-Duràn, G.A. Morris, A. Sánchez-Chardi, I. Casanova, R. Mangues, E. Vazquez, A. Villaverde, U. Unzueta, Fluorescent Dye labeling changes the Biodistribution of Tumor-Targeted Nanoparticles, Pharmaceutics 12 (2020), https://doi.org/10.3390/pharmaceutics12111004.
[14] S. Bou, F. Ng, E. Guegain, C. Peloso, A. Lopez-Noriega, M. Collot, Evaluating the in vivo stability of water-soluble PEG-PLA copolymers using FRET imaging, React. Funct. Polym. 187 (2023) 105579, https://doi.org/10.1016/j.reactfunctpolym.2023.105579.
[15] T.P. Gustafson, Y.H. Lim, J.A. Flores, G.S. Heo, F. Zhang, S. Zhang, S. Samarajeewa, J.E. Raymond, K.L. Wooley, Holistic assessment of covalently labeled core-shell polymeric nanoparticles with fluorescent contrast agents for theranostic applications, Langmuir 30 (2014) 631–641, https://doi.org/10.1021/la403943w.
[16] C. Zhu, H. Beauseroy, J. Mougin, M. Lages, J. Nicolas, In situ synthesis of degradable polymer prodrug nanoparticles, Chem. Sci. 16 (2025) 2619–2633, https://doi.org/10.1039/D4SC07746F.
[17] M.P. Monopoli, D. Walczyk, A. Campbell, G. Elia, I. Lynch, F.B. Bombelli, K. A. Dawson, Physical-chemical aspects of protein corona: relevance to in vitro and in vivo biological impacts of nanoparticles, J. Am. Chem. Soc. 133 (2011) 2525–2534, https://doi.org/10.1021/ja107583h.
[18] F. Bertoli, D. Garry, M.P. Monopoli, A. Salvati, K.A. Dawson, The Intracellular Destiny of the Protein Corona: a Study on its Cellular Internalization and Evolution, ACS Nano 10 (2016) 10471–10479, https://doi.org/10.1021/acsnano.6b06411.
[19] J. Vohlídal, Polymer degradation: a short review, Chemistry teacher, International 3 (2021) 213–220, https://doi.org/10.1515/cti-2020-0015.
[20] M.M. Perfilov, A.S. Gavrikov, K.A. Lukyanov, A.S. Mishin, Transient Fluorescence labeling: Low Affinity-High Benefits, Int. J. Mol. Sci. 22 (2021), https://doi.org/10.3390/ijms222111799.
[21] L. Arms, D.W. Smith, J. Flynn, W. Palmer, A. Martin, A. Woldu, S. Hua, Advantages and Limitations of Current Techniques for Analyzing the Biodistribution of Nanoparticles, Front. Pharmacol. 9 (2018) 802, https://doi.org/10.3389/fphar.2018.00802.
[22] T. Thomsen, A.B. Ayoub, D. Psaltis, H.-A. Klok, Fluorescence-based and Fluorescent Label-Free Characterization of Polymer Nanoparticle decorated T Cells, Biomacromolecules 22 (2021) 190–200, https://doi.org/10.1021/acs.biomac.0c00969.
[23] S. Behzadi, M. Gallei, J. Elbert, M. Appold, G. Glasser, K. Landfester, D. Crespy, A triblock terpolymer vs. blends of diblock copolymers for nanocapsules addressed by three independent stimuli, Polym. Chem. 7 (2016) 3434–3443, https://doi.org/10.1039/c6py00344c.
[24] C. Simonsson, G. Bastiat, M. Pitorre, A.S. Klymchenko, J. Béjaud, Y. Mély, J.-P. Benoit, Inter-nanocarrier and nanocarrier-to-cell transfer assays demonstrate the risk of an immediate unloading of dye from labeled lipid nanocapsules, Eur. J. Pharm. Biopharm. 98 (2016) 47–56, https://doi.org/10.1016/j.ejpb.2015.10.011.
[25] B.J. Marquis, S.A. Love, K.L. Braun, C.L. Haynes, Analytical methods to assess nanoparticle toxicity, Analyst 134 (2009) 425–439, https://doi.org/10.1039/B818082B.
[26] E. Kolomiets, J.-M. Lehn, Double dynamers: molecular and supramolecular double dynamic polymers, Chem. Commun. (Camb) (2005) 1519–1521, https://doi.org/10.1039/B418899C.
[27] Y. Liu, J.-M. Lehn, A.K.H. Hirsch, Molecular Biodynamers: Dynamic Covalent Analogues of Biopolymers, Acc. Chem. Res. 50 (2017) 376–386, https://doi.org/10.1021/acs.accounts.6b00594.
[28] L. Zeroug-Metz, S. Lee, Biodynamers: applications of Dynamic Covalent Chemistry in Single-Chain Polymer Nanoparticles, Drug Deliv, Transl. Res. 14 (2024) 3599–3607, https://doi.org/10.1007/s13346-024-01665-z.
[29] Y. Liu, M.C.A. Stuart, M.D. Witte, E. Buhler, A.K.H. Hirsch, Saccharide-Containing Dynamic Proteoids, Chemistry 23 (2017) 16162–16166, https://doi.org/10.1002/chem.201703584.
[30] S. Lee, C. Kaya, H. Jang, M. Koch, B. Loretz, E. Buhler, C.-M. Lehr, A.K.H. Hirsch, pH-dependent morphology and optical properties of lysine-derived molecular biodynamers, Mater. Chem. Front. 4 (2020) 905–909, https://doi.org/10.1039/c9qm00651f.

[31] P.P.P. Kumar, S. Saxena, R. Joshi, BODIPY Dyes: a New Frontier in Cellular Imaging and Theragnostic applications, Colorants 4 (2025) 13, https://doi.org/10.3390/colorants4020013.
[32] A. Loudet, K. Burgess, BODIPY dyes and their derivatives: syntheses and spectroscopic properties, Chem. Rev. 107 (2007) 4891–4932, https://doi.org/10.1021/cr078381n.
[33] S. Das, S. Dey, S. Patra, A. Bera, T. Ghosh, B. Prasad, K.D. Sayala, K. Maji, A. Bedi, S. Debnath, BODIPY-Based Molecules for Biomedical applications, Biomolecules 13 (2023) 1723, https://doi.org/10.3390/biom13121723.
[34] C. Kalarikkal, S. Anjali, K. Bhattacharjee, C.A.S.P. Mapa, Lipid droplet specific BODIPY based rotors with viscosity sensitivity to distinguish normal and cancer cells: impact of molecular conformation, J. Mater. Chem. B 13 (2025) 1474–1486, https://doi.org/10.1039/D4TB02405B.
[35] C. Yang, Z. Peng, L. Yang, B. Du, C. Guo, S. Sui, J. Wang, J. Li, J. Wang, N. Li, Design and application of artificial rare L-lysine codons in Corynebacterium glutamicum, Front. Bioeng. Biotechnol. 11 (2023) 1194511, https://doi.org/10.3389/fbioe.2023.1194511.
[36] S. Cong, J. Chen, L. Wang, L. Lan, Y. Wang, H. Dai, H. Liao, Y. Zhou, Y. Yu, J. Duan, Z. Li, I. McCulloch, W. Yue, Donor Functionalization Tuning the N-Type Performance of Donor–Acceptor Copolymers for Aqueous-Based Electrochemical Devices, Adv. Funct. Mater. 32 (2022) 2201821, https://doi.org/10.1002/adfm.202201821.
[37] M.A.M. Kamal, J. Bassil, B. Loretz, A.K.H. Hirsch, S. Lee, C.-M. Lehr, Arg-biodynamers as antibiotic potentiators through interacting with Gram-negative outer membrane lipopolysaccharides, Eur. J. Pharm. Biopharm. 200 (2024) 114336, https://doi.org/10.1016/j.ejpb.2024.114336.
[38] T. Ozdemir, J.L. Bila, F. Sozmen, L.T. Yildirim, E.U. Akkaya, Orthogonal Bodipy Trimers as Photosensitizers for Photodynamic Action, Org. Lett. 18 (2016) 4821–4823, https://doi.org/10.1021/acs.orglett.6b02418.
[39] S. Zheng, G. Liu, Polymeric Emissive Materials based on Dynamic Covalent Bonds, Molecules 27 (2022) 6635.
[40] Y. Liu, M.C.A. Stuart, E. Buhler, J.-M. Lehn, A.K.H. Hirsch, Proteoid Dynamers with Tunable Properties, Adv. Funct. Mater. 26 (2016) 6297–6305, https://doi.org/10.1002/adfm.201601612.
[41] A.K.H. Hirsch, E. Buhler, J.-M. Lehn, Biodynamers: self-organization-driven formation of doubly dynamic proteoids, J. Am. Chem. Soc. 134 (2012) 4177–4183, https://doi.org/10.1021/ja2099134.
[42] J.F. Folmer-Andersen, E. Buhler, S.-J. Candau, S. Joulie, M. Schmutz, J.-M. Lehn, Cooperative, bottom-up generation of rigid-rod nanostructures through dynamic polymer chemistry, Polym. Int. 59 (2010) 1477–1491, https://doi.org/10.1002/pi.2864.
[43] A.L. Parry, P.H.H. Bomans, S.J. Holder, N.A.J.M. Sommerdijk, S.C.G. Biagini, Cryo electron tomography reveals confined complex morphologies of tripeptide-containing amphiphilic double-comb diblock copolymers, Angew. Chem. Int. Ed. Engl. 47 (2008) 8859–8862, https://doi.org/10.1002/anie.200802834.
[44] Y. Wei, M.J.A. Hore, Characterizing polymer structure with small-angle neutron scattering: a Tutorial, J. Appl. Phys. 129 (2021) 171101, https://doi.org/10.1063/5.0045841.
[45] R. Ishige, Precise structural analysis of polymer materials using synchrotron X-ray scattering and spectroscopic methods, Polym. J. 52 (2020) 1013–1026, https://doi.org/10.1038/s41428-020-0357-2.
[46] L. Wang, L. Li, D. Cao, A BODIPY-based dye with red fluorescence in solid state and used as a fluorescent and colorimetric probe for highly selective detection of cyanide, Sens. Actuators B 239 (2017) 1307–1317, https://doi.org/10.1016/j.snb.2016.09.112.
[47] T. He, D. Tang, C. Lin, X. Shen, C. Lu, L. Xu, Z. Gu, Z. Xu, H. Qiu, Q. Zhang, S. Yin, Conjugated Polymers Containing BODIPY and Fluorene units for Sensitive Detection of CN− Ions: Site-Selective Synthesis, Photo-Physical and Electrochemical Properties, Polymers 9 (2017) 512, https://doi.org/10.3390/polym9100512.
[48] Z. Chen, Z. Chen, Functional supramolecular aggregates based on BODIPY and aza-BODIPY dyes: control over the pathway complexity, Org. Chem. Front. 10 (2023) 2581–2602, https://doi.org/10.1039/D3QO00148B.
[49] X. Song, X. Han, F. Yu, J. Zhang, L. Chen, C. Lv, A reversible fluorescent probe based on C–N isomerization for the selective detection of formaldehyde in living cells and in vivo, Analyst 143 (2018) 429–439, https://doi.org/10.1039/c7an01488k.
[50] W.-C. Chen, P. Venkatesan, S.-P. Wu, A turn-on fluorescent probe for hypochlorous acid based on HOCl-promoted removal of the C–N bond in BODIPY-hydrazone, New J. Chem. 39 (2015) 6892–6898, https://doi.org/10.1039/c5nj01083g.
[51] Y. Liao, A. Aspin, Z. Yang, Anaerobic oxidation of aldehydes to carboxylic acids under hydrothermal conditions, RSC Adv. 12 (2022) 1738–1741, https://doi.org/10.1039/d1ra08444e.
[52] C.S. Batsika, C. Koutsilieris, G.S. Koutoulogenis, M.G. Kokotou, C.G. Kokotos, G. Kokotos, Light-promoted oxidation of aldehydes to carboxylic acids under aerobic and photocatalyst-free conditions, Green Chem. 24 (2022) 6224–6231, https://doi.org/10.1039/D2GC02074B.
[53] E. Teknikel, C. Unaleroglu, Colorimetric and fluorometric pH sensor based on bis (methoxycarbonyl)ethenyl functionalized BODIPY, Dyes Pigm. 120 (2015) 239–244, https://doi.org/10.1016/j.dyepig.2015.04.021.
[54] H. Liu, W. Song, D. Gröninger, L. Zhang, Y. Lu, K.S. Chan, Z. Zhou, K. Rurack, Z. Shen, Real-time monitoring of newly acidified organelles during autophagy enabled by reaction-based BODIPY dyes, Commun. Biol. 2 (2019) 442, https://doi.org/10.1038/s42003-019-0682-1.
[55] R.C.R. Gonçalves, E. Belmonte-Reche, J. Pina, M. Da Costa Silva, S.C.S. Pinto, J. Gallo, S.P.G. Costa, M.M.M. Raposo, Bioimaging of Lysosomes with a BODIPY pH-dependent Fluorescent Probe, Molecules 27 (2022), https://doi.org/10.3390/molecules27228065.
[56] R. Wills, J. Farhi, P. Czabala, S. Shahin, J.M. Spangle, M. Raj, Chemical sensors for imaging total cellular aliphatic aldehydes in live cells, Chem. Sci. 14 (2023) 8305–8314, https://doi.org/10.1039/D3SC02025H.
[57] T. Komatsu, Y. Urano, Y. Fujikawa, T. Kobayashi, H. Kojima, T. Terai, K. Hanaoka, T. Nagano, Development of 2,6-carboxy-substituted boron dipyrromethene (BODIPY) as a novel scaffold of ratiometric fluorescent probes for live cell imaging, Chem. Commun. (Camb) (2009) 7015–7017, https://doi.org/10.1039/b917209b.
[58] K. Shortall, A. Djeghader, E. Magner, T. Soulimane, Insights into Aldehyde Dehydrogenase Enzymes: a Structural Perspective, Front. Mol. Biosci. 8 (2021) 659550, https://doi.org/10.3389/fmolb.2021.659550.
[59] J. Xia, S. Li, S. Liu, L. Zhang, Aldehyde dehydrogenase in solid tumors and other diseases: potential biomarkers and therapeutic targets, MedComm 4 (2023) e195.
[60] C. Godoy-Alcántar, A.K. Yatsimirsky, J.-M. Lehn, Structure-stability correlations for imine formation in aqueous solution, J. Phys. Org. Chem. 18 (2005) 979–985, https://doi.org/10.1002/poc.941.
[61] M.E. Belowich, J.F. Stoddart, Dynamic imine chemistry, Chem. Soc. Rev. 41 (2012) 2003–2024, https://doi.org/10.1039/c2cs15305j.
[62] Y. Liu, S. Ashmawy, L. Latta, A.-V. Weiss, A.F. Kiefer, S. Nasr, B. Loretz, A.K. H. Hirsch, S. Lee, C.-M. Lehr, pH-responsive Dynaplexes as Potent Apoptosis Inductors by Intracellular delivery of Survivin siRNA, Biomacromolecules 24 (2023) 3742–3754, https://doi.org/10.1021/acs.biomac.3c00424.
[63] S. Lee, S. Nasr, S. Rasheed, Y. Liu, O. Hartwig, C. Kaya, A. Boese, M. Koch, J. Herrmann, R. Müller, B. Loretz, E. Buhler, A.K.H. Hirsch, C.-M. Lehr, Proteoid biodynamers for safe mRNA transfection via pH-responsive nanorods enabling endosomal escape, J. Control. Release 353 (2023) 915–929, https://doi.org/10.1016/j.jconrel.2022.12.018.